A three-dimensional seismic velocity model for northwestern Europe

Annabel Kelly[1,2], Richard W England[1] and Peter K H Maguire[1]

[1]*Department of Geology, University of Leicester, LE1 7RH, UK. E-mail: rwe5@le.ac.uk*
[2]*Now at the US Geological Survey, Menlo Park, CA 94025, USA*

Abbreviated title: Seismic velocity model for NW Europe

Corresponding author:

Dr R. W. England
Department of Geology
University of Leicester
University Road
Leicester LE1 7RH, UK

Tel: 0116 252 3795
Fax: 0116 252 3918
E-mail: rwe5@le.ac.uk

SUMMARY

A model of the variation in seismic P-wave velocity structure in the crust of NW Europe has been compiled from existing wide-angle/refraction profiles. Along each 2D profile a velocity-depth function has been digitised at 5 km intervals. These 1D velocity functions were mapped into 3 dimensions using ordinary kriging with weights determined to minimise the difference between digitised and interpolated values. An analysis of variograms of the digitised data suggested a radial isotropic weighting scheme was most appropriate. The dimensions of the model cells were determined by applying the kringing scheme to the Moho data and minimising the misfit between calculated and observed depth to Moho. Horizontal dimensions of the model cells are optimised at 40 x 40 km and the vertical dimension at 1 km. To verify the variation in velocity indicated by the model, seismic velocities were converted to density and 3D gravity modelling was performed. After correction for long wavelength anomalies resulting from the lithosphere and asthenosphere structure, a minimised rms misfit between observed and calculated gravity anomalies of 8.8 mgals was obtained. The resulting model provides a higher resolution image of the 3D variation in seismic velocity structure of NW Europe than existing models.

1 INTRODUCTION

Models of the seismic velocity structure of the continental crust play an important role in seismology as the starting point for a variety of types of study. They can be used for improved location of earthquakes, thus assisting in defining and mitigating seismic hazards. Global models of crustal velocity structure (e.g. Bassin et al. 2000) may be used in the application of travel time corrections to teleseismic arrivals, facilitating investigation of the interior of the earth. In conjunction with earthquake data, models may be used as the starting point for crustal tomography, which in turn adds new information to the model, refining it and improving its resolution. In addition to applications in seismology, crustal models define variations in physical properties, which have applications in modelling of tectonic processes and the evolution of the continental lithosphere.

Deep seismic refraction profiles have been acquired around the world since the 1950s, providing snapshots of the crustal structure beneath the survey areas. As the quantity of data has grown numerous authors have brought together the individual surveys into global or regional compilations and used the data to map out the thickness and structure of the crust (Mooney et al. (2002) list 38 compilations of crustal structure data published between Closs and Behnke (1961) and Mooney et al. (1998)). With ever increasing quantities and quality of individual surveys, there has been a continual improvement in the detail of these models. However, the global coverage of seismic data is still quite sparse and data are very irregularly distributed, limiting the global models to coarse grid dimensions (e.g. 2 degrees for CRUST2.0 (Bassin et al. 2000)). Regional studies in densely surveyed areas allow significant refinement of the models and thus much greater detail may be included. As a result of extensive scientific research in conjunction with hydrocarbon exploration, NW Europe is unique in having relatively dense coverage by deep seismic refraction profiles over such an extensive area. In this contribution the available data in NW Europe have been compiled and digitised, building on an earlier compilation (Clegg & England 2003) for the region.

As well as controlled source profiling, a number of natural source techniques provide information on the thickness and structure of the crust, such as delay time analysis, receiver functions and tomography. However, controlled source wide-angle reflection/refraction seismic profiling (hereafter referred to as wide-angle data) offers a number of distinct advantages as a starting point for building models of the crustal velocity structure. Primarily, through modelling, wide-angle seismic data recovers true (or interval) velocity and depth to major interfaces within determinable uncertainties. Little or no a-priori information is required. In contrast, normal-incidence reflection, tomographic, delay time, and receiver

function methods suffer from the coupled uncertainty between velocity and depth to interfaces, unless a-priori constraints are available. Most wide-angle reflection experiments are conducted with particular targets in mind and hence receiver and source locations are usually planned for optimum coverage of the sub-surface. Whereas passive experiments are restricted by the range of back azimuths of those events occurring during the recording period. However, passive techniques may give a better indication of the range of anisotropy present and most refraction experiments have, to date, been 2D and hence their spatial coverage is restricted. This contribution describes the construction of a 3D model of crustal P-wave velocity structure for NW Europe (Fig. 1), based on interpolation of 2D wide-angle refraction profiles by ordinary kriging. The model is verified using potential field data and its limitations are discussed.

2 THE DATABASE

The model is built from a database that provides the input for 3 surfaces (topography/bathymetry, top basement and Moho) and 2 layers (sediments and crystalline basement), which are combined to produce the model. At the core of the model is a database of digitised wide-angle seismic profiles that provide the input data for the velocity of the crystalline basement layer and the Moho depth. The locations of the profiles included in the database are shown in Fig. 1 and a complete listing of the profiles and the primary source of the data is listed in the Appendix. Each profile was sampled at 5 km intervals to provide a suite of 1D velocity-depth functions and Moho depth information. Velocity values were initially recorded at the exact depth of nodes or boundaries beneath each surface point and then, after checking for errors, were resampled to 100 m depth intervals using linear interpolation.

Uncertainties in the velocities and Moho depths have been assigned to the wide-angle models and have been included in the database. Where available, published uncertainties have been used, but it is rare for a comprehensive review of uncertainties to be included in most published work. Consequently, experience with modelling wide-angle data and estimates based on comparable published work have been used as a guide in making qualitative uncertainty estimates. Experiments were considered comparable when they used similar source and receiver coverage and modelling methods. These two factors were the primary considerations in assessing uncertainties. Models constructed using ray tracing methods or methods in which the velocity structure is determined by travel-time tomography with the Moho included as a floating reflector (e.g. FAST, Zelt and Barton, 1998) were considered 'good'. Modelling using time term methods, T^2-X^2 and other miscellaneous methods were considered 'poor'. Simple fitting of constant velocity layers on the basis of gradient and intercept time of arrivals on record sections was considered 'very poor'. This qualitative assessment included whether the modelling was one or two dimensional, with 1D models being considered significantly poorer than 2D models. Methods based on inverse, rather

than forward, modelling were considered superior, although less emphasis was placed on this than the general modelling method. The density of data coverage (i.e. spacing of receivers and shots) and whether the survey had reversed coverage were considered almost as important to the velocity uncertainty as the modelling method. The data coverage was generally assessed through published ray path diagrams. Inspection of ray path coverage was considered particularly significant when assessing uncertainty in Moho depth as is it rare for a survey to have PmP reflections along the full length of the profile. Large sections of the Moho are often unsampled in even the best designed experiments with good data recovery (e.g. Klingelhöfer et al. 2005). Additionally the use of gravity modelling was considered to improve the uncertainty in the depth to the Moho, particularly in regions poorly constrained by PmP reflections, but to be very much secondary to the seismic modelling method and data coverage. The use of amplitude information was considered to significantly reduce uncertainties in velocities by better defining gradients in the models. The quality of the data in terms of signal to noise ratio was also examined, although not considered as significant. Within the published seismic models coincident normal incidence reflection surveys have been used in a number of ways: to construct a starting model; to constrain the sediment geometries and velocity structure; directly as additional data in the modeling; and as an independent source of data to assess the final model. When used in either the first or second approach, the normal incidence data is considered to help produce a more accurate final model, but to have little effect on the constraint/uncertainty of that model. In the third approach the data is considered during the assessment of data coverage. If used only to assess the final model the data has no effect on the constraints on velocity.

Uncertainties have generally been assigned as percentages of the velocity values and as absolute uncertainty, in kilometres, for the Moho depths. The two most common modelling methods are ray tracing and time-term analysis. Typical errors assigned to a ray traced model with good data coverage (e.g. ocean bottom recorders every 30-60 km and dense coverage of airgun shots) and consideration of amplitude data would be ~ 3% (approximately equivalent to ± 0.2 km s^{-1}) for the upper crust and ± 5 % (~ ± 0.35 km s^{-1}) at the base of the crust. The models in which time-term analysis has been used are generally older than the ray traced models and so have poorer data coverage and amplitude data is not used. As a result such models are typically assigned errors of ± 7 % (approximately equivalent to ± 0.3 km s^{-1}) for the upper crust increasing to ± 10 % (~ ± 0.6 km s^{-1}) at the base of the crust. The depths to mid-crustal interfaces were not assigned uncertainties as this information is largely redundant. In the case of first order discontinuities, the uncertainty on mid-crustal interfaces is related to the velocity step across the interface. Interfaces associated with large velocity discontinuities are generally well constrained. Only those interfaces associated with small velocity steps (or highly uncertain velocities) are poorly constrained. Therefore, where interfaces are poorly constrained the velocity step across the interface is

generally much smaller than the uncertainties in the velocity values either side. As a result the discontinuity is largely masked by the velocity uncertainties and the uncertainty on its depth becomes relatively irrelevant. A full list of the assigned uncertainties for each model is given in the Appendix.

Where the sedimentary layer is present, a 1D profile of increasing velocity with depth was used to define the velocity structure. This velocity–depth function was derived using the interval velocities calculated from stacking (rms) velocities taken from the reflection profiles listed in Table 1. These data were chosen to cover each of the major sedimentary basins in the region. The velocity data were converted to a mean velocity–depth profile by calculating a power regression curve through the median value of velocities (binned into 0.5 km depth intervals) (Fig. 2). An estimate of the uncertainties associated with the velocity of the sediments was acquired by fitting similar regression curves through the 5th and 95th percentiles of the binned data (Fig. 2). The equations that define the minimum, best-fit and maximum velocity values are: 5th percentile $v = 2.1648z^{0.2929}$; median $v = 2.909z^{0.2255}$; 95th percentile $v = 4.8018z^{0.0584}$; where v is velocity (km s^{-1}) and z is the depth below the surface/sea bed (km).

The top surface of the model is defined by the topography and bathymetry. The data used in the model were extracted from the Smith & Sandwell (1997) bathymetry and GTOPO30 topography.

The interface between the sediments and crystalline crust was compiled from a number of data sources. For much of the model the NGDC map of "Sediment Thickness in the World's Oceans and Marginal Seas" (National Geophysical Data Center 2004) defines the surface. This map was not used in the North Sea as it follows the base of the Mesozoic syn-rift sediments and does not include the significant thickness of pre-rift Permian sediments in the region. In the North Sea top basement picks in the BIRPS reflection data (Klemperer and Hobbs 1991) were converted to depth using an empirically derived velocity function based on a conversion of stacking (rms) to interval velocities and high resolution wide-angle data. These profiles were then extrapolated using the tensioned minimum curvature algorithm of Smith & Wessel (1990). For onshore Britain a digital version of the Variscan unconformity was provided by the British Geological Survey and was used to define the base of the sediments. These data are also published in Whittaker (1985). In regions not covered by the datasets described above, the base of the sediments was taken from a 1 degree resolution, global map of sediment thickness (Laske & Masters 1997). The only exceptions are Scotland, Ireland and Brittany where the sediment thicknesses were set to zero as the 1 degree resolution results in artificial sediment thickness in regions of short-wavelength topographic change.

3 CONSTRUCTION OF THE VELOCITY MODEL

The model is defined using Cartesian coordinates, with distances measured in kilometers, based on a Transverse Mercator projection centred at 3.4º west, 57.15º north. The velocity structure of the crystalline crust was constructed by interpolation of the digitised wide-angle seismic data assuming that the data were a randomly distributed set of points. This assumption fails in the direction of the profiles but is valid between profiles in the areas in which the velocity is to be interpolated, since the majority are not arranged on a regular gird. The interpolation method was 3D ordinary kriging using the Deutsch and Journal (1998) code KT3D. The Moho surface was also built primarily through ordinary kriging using KT3D. However, the regions around the Porcupine Bank, Biscay Margin and the Shetland Islands were adjusted after gravity modelling, discussed below. Kriging assumes that the spatial autocorrelation of the variable (in this case velocity or Moho depth) is known in the form of the semivariogram or covariance, and uses this to weight data points and estimate the value of the variable away from the known sample locations. This use of the statistical model, based on the data, to produce the weights for the interpolation makes kriging a superior technique compared to traditional methods, such as inverse distance interpolation, which use a weighting function that may not be appropriate for the data. The spatial continuity of the variable is described by the variogram model. The models used for the interpolation of the velocity and Moho data were based on experimental variograms of the input data (Figs 3 and 4). These experimental variograms have been inspected to assess anisotropy, range, near origin behaviour and structure at intermediate lags.

3.1 Anisotropy

For both the Moho and velocity data sets the experimental variograms show evidence for anisotropy. In the Moho data there is zonal anisotropy, i.e. a direction dependent sill but constant range, with a minimum sill in a NE or NNE direction (Fig. 3a). Such a trend is likely to be inherited from the relatively high sampling of the continental margin between Hatton Bank and the Lofoten Islands. Along this margin the topography and Moho depths show the rapid change in the NW direction associated with the transition from continent to ocean, but far greater continuity in the NE direction, parallel to the margin (Fig. 1). It is also possible that the NE-NNE structural trend generated during the Caledonian Orogeny has some residual signature affecting the Moho data away from the continental margin. However, as the anisotropy is probably restricted to the northwest European continental margin, the risk of over-interpreting and introducing erroneous structure into the interpolated Moho surface was considered too high to include anisotropy in the model.

The velocity data show unquestionable dip-dependent zonal and geometric anisotropy, i.e. dip dependent sill and range, with the horizontal variograms exhibiting greater ranges and lower sills than the dipping variograms (cf Figs 4a, 4b and 4c). This is consistent with what is known of the crustal velocity structure from 2D models. A vertical profile through the crust may well show increasing velocity from 5 km s^{-1} to 7 km s^{-1} over a few 10s of kilometers depth, whereas the horizontal variation may well be less than 1 km s^{-1} along a 2D profile several hundred kilometers in length. Therefore, the horizontal variation is expected to be both smaller in magnitude and spatially less rapidly changing than the vertical variation. There is no clear evidence for azimuth-dependent anisotropy. Therefore, the model variogram was constructed to reproduce the dip-dependent zonal and geometric anisotropy, but to be azimuthally isotropic.

3.2 Sill and Range

The experimental semivariogram for the Moho data shows a well-developed sill with a range of approximately 800 km (Fig. 3b). For the velocity data the horizontal variograms show a well-developed sill, at ~ 0.5 km^2 s^{-4}, beyond a range of approximately 150 km. The sill for the dipping variograms is not well developed, but is higher than 0.5 km^2 s^{-4}. The best fit curve to the dipping variograms suggests a model with a vertical range of 35 km and sill of 1.2 km^2 s^{-4} (Figs 4a, 4b and 4c).

3.3 Near-origin behaviour

Variables that are highly continuous over short distances, such as depth or layer thickness data, usually exhibit parabolic behaviour near the origin of the variogram. As adjacent points on a continuous surface will be at almost identical height the variability at short lags is very small. Such surfaces are often modelled with a Gaussian weighting function to reproduce this continuity. However, there is no evidence for this behaviour in the Moho data, which are approximately linear at the origin (Figs 3a and 3b). It is highly likely that the experimental variograms are affected by the mismatches in the Moho depth at profile intersections, increasing the variability between closely spaced data (this is certainly the cause for the reduction in continuity at the shortest lag). Even if such effects are concealing what would otherwise be parabolic behaviour, with no data to constrain a parabolic curve it is unreasonable to try and fit a Gaussian model to the data. Instead a model with linear behaviour near the origin was considered more appropriate. For all the velocity variograms the short lags show near linear behaviour (Figs 4a, 4b and 4c). This is consistent with the observation that the velocity structure can contain discontinuities and rapid changes within the crust.

3.4 Structure at intermediate lags

A transitional model (i.e. including a sill) with near linear behaviour near the origin is required for oth the Moho depth and crustal velocity data (as described above). The two most common transitional models are the spherical model and the exponential model. The models are broadly similar, differing only in the rate of change. As the Moho experimental semivariogram (Fig. 3b) and correlogram (Fig. 3c) show reasonably linear behaviour at the intermediate lags, the spherical model was preferred to the exponential model. For the velocities, the dipping variograms show reasonably smooth variation at intermediate lags. However, the horizontal variograms have a sharp change in gradient at a lag of approximately 50 km. This sharp change is reproduced by adding a second horizontal structure with a short range to cause the initial rapid increase, but which keeps the horizontal range at 150 km.

The final variogram structure chosen to model the Moho data was a single, isotropic spherical structure with a range of 800 km and sill of 49 km^2 (Fig. 3b), The velocity variogram model consists of three structures: A spherical structure with a 50 km horizontal range, 35 km vertical range and 0.2 km^2 s^{-4} sill; a spherical structure with a 150 km horizontal range, 35 km vertical range and 0.3 km^2 s^{-4} sill; and a further spherical structure with infinite horizontal range, 35 km vertical range and 0.7 km^2 s^{-4} sill.

3.5 Dimensions of the model elements

To determine the optimum spatial dimensions of the model elements the Moho data were interpolated onto a range of grids. Investigation of the model dimension was based on the Moho data, rather than the velocity data, in order to save computational time. Given the similarity between the Moho and velocity distributions (Fig. 1), and that velocity data were interpolated with very little weight allocated to data at different depths, using 2D data instead of 3D data has very little impact on the evaluation of model parameters. In order to assess the model quality the kriging uncertainty was recorded for results of the interpolation onto each of a range of grid sizes. The preferred grid has dimensions that minimise the rms uncertainty, recorded as variance. The results of interpolations onto grids with cell sizes ranging between 10–80 km show that the kriging uncertainty is relatively insensitive to the model dimensions. However, 40 km cells minimise the variance (Fig. 5). The vertical element size was set to reflect the balance between the desire to have fine spacing to reproduce the vertical variation seen in the input data and the need to have coarser spacing to allow for the poorer resolution of the velocity structure in the lower crust (Section 2). The Moho uncertainties, which have an average of ~2 km, give an indication of the depth resolution in the lower crust. However, given that the resolution in the upper crust is significantly greater and that lower crustal velocity gradients are generally small, a vertical element dimension of 1 km was considered the most appropriate for the crustal layer as a whole.

The search parameters used in the final model required a minimum of 25 and maximum of 64 data points, with the maximum per octant of 8. The search radius was set to 800 km, allowing Moho depths to be estimated at all constrained locations. The limits of the Moho estimation define the model boundaries. The same search range was used for the velocity data, ensuring that all cells within the model would be assigned a Moho depth and velocity.

The kriged velocity data was combined with the sediment velocity estimates, with the layer thicknesses defined using the interpolated Moho (Fig. 6) and filtered versions of the topography and base-sediment surfaces. The interface between the sediment and crystalline layers in general falls within one of the model cells (rather than falling exactly at the cell boundary). Therefore, to reproduce the velocity structure as accurately as possible, the cell containing the base-sediment interface is assigned a weighted average of the sediment and crystalline crust velocities. The weighting is controlled by the fraction of the cell containing sediment and the fraction containing crystalline crust.

To obtain total uncertainty in the velocity of each model cell and the Moho depth, the uncertainties in the database were combined with the kriging uncertainties using the law of propagation of errors. Two assumptions were made in doing this. First, the uncertainty associated with the input data conforms to a Gaussian distribution. Second, the database uncertainties are equal to twice the standard deviation in the data. The uncertainties are likely to have a skewed, rather than normal, distribution; however, assessing the skew for each data point is impossible. Additionally, an analysis of uncertainties from modelling the MONA LISA wide-angle profile crossing the Southern North Sea (Kelly 2006) suggests that the assumption of a Gaussian distribution is not unreasonable. The Moho uncertainties are shown in Fig. 6 and the velocity uncertainties are shown alongside depth slices through the final model in Fig. 10.

4 GRAVITY MODELLING

In order the verify the model the interpolated seismic velocities of the crystalline crust were converted to density using the linear equations of Christensen and Mooney (1995). Of the published velocity–density relationships this is the most applicable to this work as it is specifically aimed at characterising continental crust. The regression equation is based on a large number of velocity and density values measured in a range of crustal rocks at appropriate temperatures and pressures for the continental crust. The model was then transformed into a simplified 4 layered model for input into the British Geological Survey's Gmod 3D gravity modelling package (Dabek and Williamson 1999). The sediments were divided into two layers, with densities calculated using a standard compaction curve (Sclater and Christie 1980). The other two layers form the crystalline crust, with the 40 km lateral variation preserved and the

density assigned from the mean values of the column of model cells that fall into each layer. The calculated gravity anomaly was compared with the 2 minute satellite derived Free-Air anomaly (Sandwell and Smith, 1997) after a long wavelength component of the gravity field was calculated and deducted from the observed data to account for the proximity of the relatively young Atlantic continental margin (O'Reilly et al. 1998) and lateral density variation in the sub-continental mantle (Fig. 7). In general, the uncertainty in the velocity-density relationship is great enough to permit alteration of the densities to match the gravity anomalies (Fig. 8). However, in regions around the Porcupine Bank and Trough, the north Biscay continental Margin and under the Shetland Islands, matching the observed gravity anomaly required a change in the depth of the Moho (Fig. 9). In these regions the seismic data control is such that relief on the Moho that is similar in structure and relative amplitude to the topographic change, could not be predicted by the interpolation. The revised Moho depth contours echo the topography and remove the misfit between observed and calculated gravity anomalies. The velocity model was rebuilt using the revised Moho depths. Depth slices though the final model and the mean velocity of the model are shown in Figs 10 and 11.

5 PRINCIPAL FEATURES OF THE MODEL

The variogram model of the velocity data has a relatively short range compared to the profile spacing and this is shown in the plots of velocity uncertainty (Fig. 10). As a result of the short variogram range the velocity constraint diminishes rapidly away from the data points, resulting in uncertainty maps that, once below the sediment layers, clearly mimic the data distribution. Consequently, for much of the model space the calculated velocities represent a best estimate. It also indicates the density of data required for this method of model construction to produce a well-constrained model for the whole region. The high uncertainties do not necessarily mean that the mapped velocities are inaccurate, just that they are poorly constrained.

For the top few kilometers, the model shows significant lateral velocity variation associated with the sedimentary basins (Fig. 10). By 6-7 km depth much of the model has standard upper-crustal velocities (~6 km/s), but the continuation of the deeper parts of the basins to this depth still results in lateral variations. At depths greater than 10 km the model represents the lower crust in the northwest, near the continental margin. As a result the velocities are higher in the northwest and the model shows a notable lateral velocity gradient. At greater depths increasingly large sections of the model lie in the mantle (e.g. along the continental margins and under the Celtic Sea) and in the lower crust elsewhere. The lower crust on the northwest side of the North Sea Central Graben shows higher velocities than the southeast.

Elevated velocities are also seen under Ireland and particularly the Irish Sea, a region of possible magmatic underplating (Al-Kindi et al. 2003; Shaw Champion et al. 2006; Tomlinson et al. 2006).

The largest lateral variations in the velocity structure in the model are associated with the sedimentary basins (Figs 1 and 10). This is also shown by the mean crustal velocity map (Fig. 11a). However, removing the sediments from the mean velocity calculation (Fig. 11b) illustrates that there are also variations in the velocity structure of the crystalline crust. Most notable are the higher average velocities recorded in regions where magmatic underplating is postulated to have occurred, especially along the northwestern ocean-continent transition. The median, mean and standard deviation of the crustal velocities are 6.234, 6.173 and 0.355 respectively when including the sediment, and 6.419, 6.422 and 0.147 when using the crystalline crust only.

6 COMPARISON TO EXISTING MODELS

The most widely used crustal velocity model is the CRUST2.0 global 2° model of Bassin et al. (2000). To assist the comparison between the model presented here and the CRUST2.0 model, the average velocity structure and Moho depth of the CRUST 2.0 model are shown in Fig. 12. The median, mean and standard deviation in crustal velocities of the CRUST2.0 model in the same region as the new model are 6.255, 6.244 and 0.214 respectively, including sediment, or 6.557, 6.500 and 0.111 excluding the sediment. The most obvious difference between the models is the significant refinement in cell size for the new model, which results in far greater detail. This is most apparent for the marine sedimentary basins, for example the Rockall and North Sea basins are only poorly resolved in the CRUST2.0 model, but are well defined in the new model. Comparing the average crustal velocities, the new model has a greater range of values, both for the low velocity end of the range and the high velocity end. Some of this effect is due to smearing of the low velocity sedimentary basins in the coarser CRUST2.0 model. However, most of the difference comes from the shallow marine areas around Britain and Ireland, which are defined using a continental shelf type section in the CRUST2.0 model. This type section has higher velocities than the model presented here. As the new model is based on seismic profiles, rather than a general type section, it is more consistent with the measured velocity structure in these regions.

The Moho used to define the base of the model can be compared to the most recent published Moho map of Western Europe (Dèzes and Ziegler 2001) (Fig. 13). The two maps are very similar for much of the area covered, particularly under the Southern North Sea, Britain and Ireland. One area of notable

difference between the two maps is the Northern North Sea, where the Dezes and Ziegler map predicts significant Moho relief under the Shetland Platform and Viking Graben. This Moho structure is not seen in the model as there is no wide-angle seismic data across this region to image such relief. However, crustal scale normal incidence data in the region does suggest that there is significant Moho uplift under the Viking Graben. Therefore, this area of the model could benefit from further modelling using constraints provided by depth converted normal incidence seismic data.

7 CONCLUSIONS

We believe the model presented here is uniquely detailed for such a large region. The resolution and details of the Moho are similar to existing crustal thickness maps. However, unlike these earlier maps, the work presented here is a true crustal model, recording lateral and vertical variations in velocity structure as well as crustal thickness. This model is unique in that it includes estimations of the uncertainties in the velocity structure and crustal thickness. The velocity structure of the new model is broadly similar to the existing models, but velocities are slightly slower than in the CRUST2.0 model (Bassin et al. 2000). These lower average crustal velocities reflect a more detailed record of the sedimentary basins and the determination of velocity based on seismic profiles, rather than general type sections. However, the model would benefit from increased data coverage.

REFERENCES

Abramovitz, T. & Thybo, H., 1998. Seismic structure across the Caledonian Deformation Front along MONA LISA profile 1 in the southeastern North Sea. *Tectonophysics*, **288**, 153–176.

Abramovitz, T. & Thybo, H., 2000. Seismic images of Caledonian, lithosphere-scale collision structures in the southeastern North Sea along MONA LISA profile 2. *Tectonophysics*, **317**, 27–54.

Aichroth, B., Prodehl, C. & Thybo, H., 1992. Crustal structure along the central segment of the EGT from seismic-refraction studies. *Tectonophysics*, **207**, 43–64.

Al Kindi, S., 2002. *A seismic study of Cenozoic Epeirogoeny across the British Isles*. Ph.D. thesis, University of Cambridge, Cambridge, UK.

Al-Kindi, S., White, N., Sinha, M., England, R & Tiley, R., 2003. Crustal trace of a hot convective sheet. *Geology*, **31**, 207-210.

AMP Exclusive Report 99/3/1, 1999. *2-D Near Normal Incidence Deep Seismic Reflection profiling Phase 1: Rockall Trough*. Unpublished.

AMP Exclusive Report 01/3/3, 2001. *2-D Near Normal Incidence Deep Seismic Reflection and Wide-angle/Refraction profiling Phase2: Faroe-Shetland Trough and Shetland Platform*. Unpublished.

Avedik, F., Berendsen, D., Fucke, H., Goldflam, S., Hirschleber, H., Meissner, R., Sellevoll, M. & Weinrebe, W., 1984. Seismic investigation along the Scandinavian << Blue Norma >> profile. *Ann. geophys.,* **2**, 571–578.

BABEL working group, 1993. Deep seismic reflection/refraction interpretation of crustal structure along BABEL profiles A and B in the southern Baltic Sea. *Geophys. J. Int.*, **112**, 325–343.

Bamford, D., Faber, S., Jacob, B., Kaminski, W., Nunn, K., Prodehl, C., Fuchs, K., King, R. & Willmore, P., 1976. A Lithospheric Profile in Britain – I Preliminary Results. *Geophys. J. R. astron. Soc.*, **44**, 145–160.

Barton, A. J. & White, R. S., 1997. Crustal structure of the Edoras Bank continental margin and mantle thermal anomalies beneath the North Atlantic. *J. geophys. Res.*, **102**, 3109–3129.

Barton, P. & Wood, R., 1984. Tectonic evolution of the North Sea basin: crustal stretching and subsidence. *Geophys. J. R. astron. Soc.*, **79**, 987–1022.

Barton, P. J. 1986. The relationship between seismic velocity and density in the continental crust. *Geophys. J. R. astron. Soc.*, **87**, 195–208.

Barton, P. J., 1992. LISPB revisited: a new look under the Caledonides of northern Britain. *Geophys. J. Int.*, **110**, 371–391.

Bassin, C., Laske, G., & Masters, G., 2000. The current limits of resolution for surface wave tomography in North America. *EOS Trans. Am. geophys. Un.*, **81**, F897.

Berndt, C., Mjelde, R., Planke, S., Shimamura,H. & Faleide, J., 2001. Controls on tectonomagmatic evolution of a volcanic transform margin: the Voring Transform Margin, N E Atlantic. *Marine and Petroleum Geology*, **22**, 133–152.

Blundell, D. J. & Parks, R., 1969. A study of the crustal structure beneath the Irish Sea. *Geophys. J. R. astron. Soc.*, **17**, 45–62.

Bott, M. H. P., Armour, A. R., Himsworth, E., Murphy, T. & Wylie, G., 1979. An explosion seismology investigation of the continental margin west of the Hebrides, Scotland, at 58 degrees N. *Tectonophysics*, **59**, 217–231.

Brooks, M., Doody, J. J. & Al-Rawi, F. R. J., 1984. Major crustal reflectors beneath SW England. *J. geol. Soc. Lon.*, **141**, 97–103.

Bunch, A.W.H., 1979.A detailed seismic structure of the Rockall Bank (55 degrees N, 15 degees W) - A synthetic seismogram analysis. *Earth planet. Sci. Lett.*, **45**, 453–463.

Christensen, N. I. & Mooney, W. D., 1995. Seismic velocity structure and composition of the continental crust. *J. geophys. Res.,* **100**, 9761-9788.

Christie, P. A., 1982. Interpretation of refraction experiments in the North Sea. *Phil Trans R Soc London*, **305**, 101–112.

Clegg, B. & England, R., 2003. Velocity structure of the UK continental shelf from a compilation of wide-angle and refraction data. *Geol. Mag.,* **140**, 4537-467.

Closs, H. & Behnke, C., 1961. Fortschritte der Anwendung seismischer Methoden in der Erforschung der Erdkruste. *Geologische Rundschau*, **51**, 315.

Dabek, Z. K. & Williamson, J. P., 1999. Forward and inverse wavenumber formulae for the gravity and magnetic responses of layered models. *British Geological Survey technical report*, WK/99/03C.

Deutsch, C. V. & Journal, A. G.,1998. *GSLIB - Geostatistical software library and user's guide*. Oxford University Press, Oxford.

Dèzes, P. & Ziegler, P., 2001. European map of Mohorovicic discontinuity, version 1.3. *http://comp1.geol.unibas.ch*.

Eldholm, O. & Grue, K., 1994. North Atlantic volcanic margins: Dimensions and production rates. *J. geophys. Res.*, **99**, 2955–2968.

EUGENO-S working group, 1988. Crustal structure and tectonic evolution of the transition between the Baltic shield and the North German Caledonides (the EUGENO-S project). *Tectonophysics*, **150**, 253–348.

Ginzburg, A., Whitmarsh, R. B., Roberts, D. G., Montadert, L., Camus, A. L. & Avedik, F., 1985. The deep seismic structure of the northern continental margin of the Bay of Biscay. *Ann. geophys.*, **3**, 499–510.

Goldschmidt-Rokita, A., Sellevoll, M. A., Hirschleber, H. B. & Avedik, F., 1988. Results of two seismic refraction profiles off Lofoten, Northern Norway. *Norges. geologiske. undersøkelse*. Special Publication., **3**, 49–57.

Grandjean, G., Guennoc, P., Recq, M. & Andreo, P., 2001. Refraction/wide-angle reflection investigation of the Cadomian crust between northern Brittany and the Channel Islands. *Tectonophysics*, **331**, 45–64.

Hauser, F., O'Reilly, B .M., Jacob, A. W. B., Shannon, P. M., Makris, J. & Vogt, U., 1995. The crustal structure of the Rockall Trough: Differential stretching without underplating. *J. geophys. Res*., **100**, 4097–4116.

Hodgson, J. A., 2002. *A seismic and gravity study of the Leinster Granite: SE Ireland.* Ph.D. thesis, University College Dublin, Dublin, Ireland.

Holder, A. P. & Bott, M. H. P., 1971. Crustal structure in the vicinity of south-west England. *Geophys. J. R. astron. Soc.,* **23**, 465–489.

Horsefield, S.J., Whitmarsh, R. B., White, R. S. & Sibuet, J.-C., 1994. Crustal structure of the Goban Spur rifted continental margin, NE Atlantic. *Geophys. J. Int*., **119**, 1–19.

Jones, E. J. W., White, R. S., Hughes, V .J., Matthews, D. H. & Clayton, B. R., 1984. Crustal structure of the continental shelf off northwest Britain from two-ship seismic experiments. *Geophysics*, **49**, 1605–1621.

Kelly, A., 2006. *The Crustal Velocity and Density Structure of Northwest Europe: A 3D Model and its Implications for Isostasy*. PhD Thesis, University of Leicester, Leicester, UK.

Klemperer, S. & Hobbs, R., 1991. *The BIRPS Atlas: Deep seismic reflection profiles around the British Isles*. Cambridge University Press.

Klingelhofer, F., Edwards, R.A., Hobbs, R.W. & England, R.W., 2005. Crustal structure of the NE Rockall Trough from wide-angle seismic data modeling. *J. geophys. Res*., **110**, doi:10.1029/2005JB003763.

Landes, M., Prodehl, C., Hauser, F., Jacob, A.W.B. & Vermeulen, N. J., 2000. VARNET96: influence of the Variscan and Caledonian orogenies in crustal structure in SW Ireland. *Geophys. J. Int*., **140**, 660–676.

Laske, G. & Masters, G., 1997. A global digital map of sediment thickness. *EOS Trans. Am. geophys. Un.,* **78**, F483.

Lowe, C. & Jacob, A.W.B., 1989. A north-south seismic profile across the Caledonian Suture zone in Ireland. *Tectonophysics*, **168**, 297–318.

Masson, F., Jacob, A. W. B., Prodehl, C., Readman, P. W., Shannon, P M., Schulze, A. & Enderle, U., 1998. A wide-angle seismic traverse through the Variscan of southwest Ireland. *Geophys. J. Int.*, **134**, 689–705.

Matte, P. & Hirn, A., 1988. Seismic signature and tectonic cross section of the Variscan crust in western France. *Tectonics*, **7**, 141–155.

McCaughey, M., Barton, P.J. & Singh, S.C. 2000. Joint inversion of wide-angle seismic data

and a deep reflection profile from the central North Sea. Geophys. J. Int., 141, 100–114.

Mjelde, R., Kodaira, S., Shimamura, H., Kanazawa, T., Shiobara, H., Berg, E. W. & Riise, O., 1997. Crustal structure of the central part of the Vøring Basin, mid-Norway margin, from Ocean Bottom Seismographs. *Tectonophysics*, **277**, 325–257.

Mjelde, R., Digranes, P., Shimamura, H., Shiobara, H., Kodaira, S., Brekke, H., Egebjerg, T., Soerenes,N. & Thorbjoernsen, T., 1998. Crustal structure of the northern part of the Vøring Basin, mid-Norway margin, from wide-angle seismic and gravity data. *Tectonophysics*, **293**, 175–205.

Mjelde, R., Digranes, P., Van Schaack, M., Shimamura, H., Shiobara, H., Kodaira, S., Naess, O., Sorenes, N. & Vaagnes, E., 2001. Crustal structure of the outer Vøring Plateau, offshore Norway, from ocean bottom seismic and gravity data. *J. geophys. Res*., **106**, 6769–6791.

Mooney, W. D., Laske, G. & Masters, G., 1998. CRUST 5.1: A global crustal model at 5 degrees x 5 degrees. *J. geophys. Res.*, **103**, 727–747 .

Mooney, W. D., Prodehl, C. & Pavlenkova, N. I., 2002. Seismic velocity structure of the continental lithosphere from controlled source data, *in International Handbook of Earthquake and Engineering Seismology,* **81A**, pp. 887–908, The International Association of Seismology and Physics of the Earth's Interior.

Morewood, N. C., Mackenzie, G. D., Shannon, P. M., O'Reilly, B. M., Readman, P. W. &Makris, J., 2005. The crustal structure and regional development of the Irish Atlantic margin region. *In Petroleum Geology: North-West Europe and Global Perspectives - Proceedings of the 6th Petroleum Geology Conference*, pp. 1023–1033, ed. Doré, A. G. & Vining, B. A., The Geological Society, London.

Morgan, J. V., Barton, P. J. & White, R. S., 1989. The Hatton Bank continental margin - III. Structure from wide-angle OBS and multichannel seismic refraction profiles. *Geophys. J. Int.*, **98**, 367–384.

Morgan, R. P. Ll., Barton, P. J., Warner, M., Morgan, J., Price, C. & Jones, K., 2000. Lithospheric structure north of Scotland-I. P-wave modelling, deep reflection profiles and gravity. *Geophys. J. Int.*, **142**, 716–736.

National Geophysical Data Center., 2004. Total sediment thickness of the World's Oceans and Margin Seas. */http://wwww.ngdc.noaa.gov/mgg/sedthick/sedthick.html.*

O'Reilly, B. M., Hauser, F., Jacob, A. W. B., Shannon, P. M., Makris, J. & Vogt, U., 1995. The transition between the Erris and the Rockall basins: new evidence from wide-angle seismic data. *Tectonophysics*, **241**, 143–163.

O'Reilly, B. M., Readman, P. W., & Hauser, F., 1998. Lithospheric structure across the western Eurasian plate from a wide-angle seismic and gravity study: evidence for a regional thermal anomaly. *Earth planet. Sci. Lett.,* **156**, 275-280.

Pearse, S., 2002. *Inversion and Modelling of Seismic Data to Assess the Evolution of the Rockall Trough*. Ph.D. thesis, University of Cambridge, Cambridge, UK.

Powell, C. M. R. & Sinha, M. A., 1987. The PUMA experiment west of Lewis, U.K. *Geophys. J. R. astron. Soc.,* **89**, 259–264.

Rabbel, W., Forste, K., Schulze, A., Bittner, R., Rohl, J. & Reichert, J. C., 1995. A high-velocity layer in the lower crust of the North German Basin. *Terra Nova*, **7**, 327–227.

Raum, T., 2003. *Crustal structure and evolution of the Faeroe, Møre and Vøring margins from wide-angle seismic and gravity data*. Ph.D. thesis, University of Bergen, Norway.

Raum, T., Mjelde, R., Digranes, P., Shimamura, H., Shiobara, H., Kodaira, S., Haatvedt, G., Sorenes, N. & Thorbjornsen, T., 2002. Crustal structure of the southern part of the Vøring Basin, mid-Norway margin, from wide-angle seismic and gravity data. *Tectonophysics*, **355**, 99–126.

Richardson, K. R., 1997. *Crustal Structure around the Faroe Islands*. Ph.D. thesis, University of Cambridge, Cambridge, UK.

Richardson, K. R., White, R. S., England, R. W. & Fruehn, J., 1999. Crustal structure east of the Faroe islands: mapping sub-basalt sediment using wide-angle seismic data. *Petroleum Geoscience*, **5**, 161-172.

Roberts, D. G., Ginzburg, A., Nunn, K. & McQuillin, R., 1988. The structure of the Rockall Trough from seismic refraction and wide-angle reflection measurements. *Nature*, **332**, 632–635.
Sandwell, D. T. &. Smith, W. H. F., 1997. Marine gravity anomaly from Geosat and ERS 1 satellite altimetry. *J. geophys. Res.,* **102**, 10039-10054.

Sapin, M. & Prodehl, C., 1973. Long range profiles in western Europe I. - Crustal structure between the Bretagne and the Central Massif of France. *Annales de Geophysique*, **29**, 127–145.

Sclater, J. G. & Christie, P. A. F. , 1980. Continental stretching: An explanation of the post-mid-Cretaceous subsidence of the central North Sea Basin. *J. geophys. Res.,* **85**, 3711-3739.

Sellevoll, M. A. & Warrick, R. E., 1971. A refraction study of the crustal structure of southern Norway. *Bull. Seis. Soc. Am.*, **61**, 457–471.

Shaw Champion, M. E., White, N. J., Jones, S. M. & Preistley, K. F., 2006. Crustal velocity structure of the British Isles; a comparison of receiver functions and wide-angle seismic data. *Geophys. J. Int*., **166**, 795-813.

Smith, P.J. & Bott, M.H.P., 1975. Structure of the crust beneath the Caledonian Foreland and Caledonian Belt of the north Scottish shelf region. *Geophys. J. R. astron. Soc.* **40**, 187–205.

Smith, W. H. F. & Wessel, P., 1990. Gridding with continuous curvature splines in tension. *Geophysics,* **55**, 293-305.

Smith, W. H. F. & Sandwell, D. T., 1997. Global sea floor topography from satellite altimetry and ship depth soundings. *Science,* **277,** 1956-1962.

Thinon, I., Matias, L., Rehault, J. P., Hirn, A., Fidalgo-Gonzalez, L. & Avedik, F., 2003. Deep structure of the Armorican Basin (Bay of Biscay): A review of Norgasis seismic reflection and refraction data. *J. geol. Soc. Lon.,* **160**, 99–116.

Thybo, H. & Schonharting, G., 1991. Geophysical evidence for early Permian igneous activity in a transtensional environment, Denmark. *Tectonophysics*, **189**, 193–208.

Tryti, J. & Sellevoll, M. A., 1977. Seismic crustal study of the Oslo rift. *Pure appl. Geophys.*, **115**, 1061–1085.

Tomlinson, J. P., Denton, P. Maguire, P. K. H. & Booth, D. C., 2006. Analysis of the crustal velocity structure of the British Isles using teleseismic receiver functions. *Geophys. J. Int.*, **167**, 223-237.

Vogt, U., 1993. *Der europäische Kontinentalsockel westlich von Irland abgeleitet aus tiefenseismischen Untersuchungen.* Reihe C: Geophysik, Zentrum fur Meeres-und Klimaforschung der Universität Hamburg.

Vogt, U., Makris, J., O'Reilly, B. M., Hauser, F., Readman, P. W., Jacob, A. W. B. & Shannon, P. M., 1998. The Hatton Basin and continental margin: Crustal structure from wide-angle seismic and gravity data. *J. geophys. Res.*, **103**, 12545–12566.

Wessel, P. & Smith, W. H. F., 1998. New improved version of Generic Mapping Tools released. *EOS Trans. Am. geophys. Un.*, **79**, 579.

Whitmarsh, R. B., Langford, J. J., Buckley, J. S., Bailey, R. J., & Blundell, D., 1974. The crustal structure beneath the Porcupine Ridge as determined by explosion seismology. *Earth planet. Sci. Lett.*, **22**, 197–204.

Whittaker, A., 1985. *Atlas of onshore sedimentary basins in England and Wales*. London, Blackie.

Zelt, C. & Barton, P., 1998. Three-dimensional seismic refraction tomography: A comparison of two methods applied to the Faeroes Basin. *J. geophys. Res.,* **103**, 7187-7210.

Figure Captions

Figure 1. Map showing the locations of wide-angle profiles entered into the database (Numbers on seismic profiles refer to the listing in the Appendix). Blue lines and points are crustal velocity data only; red lines and points are crustal velocity and Moho depth data.

Figure 2. Interval velocities plotted against depth for sedimentary basins from nine seismic profiles from around the UK (see Table 1 for line locations). Solid black line is the median velocity-depth function; broken lines are the minimum and maximum velocity-depth functions.

Figure 3. Experimental and model variograms for the Moho depth data. In each case spatial variability is plotted against lag. Range is the maximum lag over which the data shows spatial continuity. The sill is the maximum level of variation in the correlated data.

a) Semimadogram for the Moho. Black indicates a sample direction of North, red indicates a direction of 045º, green indicates a direction of 090º and blue indicates 135º.

b) Omnidirectional semivariogram for the Moho. The red line is the curve used to construct the model.

c) Omnidirectional correlogram for the Moho.

Figure 4. Experimental and model variograms for the crystalline crust velocity data. In each case spatial variability is plotted against lag. Range is the maximum lag over which the data shows spatial continuity. The sill is the maximum level of variation in the correlated data.

a) Semivariogram for the crust derived from a search in the horizontal plane through the model space. Black line is the best fit curve to the experimental data. Legend shows direction in degrees from North.

b) Semivariogram for the crust derived from a search in a plane dipping at 30º through the model space. Black line is the best fit curve to the experimental data. Legend shows direction in degrees from North.

c) Semivariogram for the crust derived from a search in a plane dipping at 60º through the model space. Black line is the best fit curve to the experimental data. Legend shows direction in degrees from North.

Figure 5. Histogram illustrating rms kriging variance against change in grid cell size, indicating an optimum horizontal cell dimension of 40 km.

Figure 6. Interpolated surface representing the Moho (a) and uncertainty in Moho depth (b). Final Moho shown in Fig. 9.

Figure 7. a) Observed Free Air Gravity (Smith and Sandwell 1998) and b) the gravity anomaly calculated from the best fit model as described in the text.

Figure 8. Velocity-density relationships for the final model, showing the individual cells of the velocity model compared to the density model. The black lines indicate the upper and lower bounds of the Nafe-Drake velocity–density pairs (Barton, 1986), the blue lines the Christensen and Mooney (1995) velocity-density functions for 10 to 40 km (the gradient decreases with depth).

Figure 9. Final Moho depth, optimised after gravity modelling.

Figure 10. Depth slices through the final crustal velocity model, the depth of the slice (in kilometers below sea level) is given in the caption. Pale grey regions are outside the model area, dark gray elements are either below the Moho or above the topography and therefore do not contain velocity data.

Figure 11. Mean crustal velocity. The left-hand image a) is the mean velocity of the entire crust including sediments, the right-hand image b) is the mean velocity of the crystalline crust only.
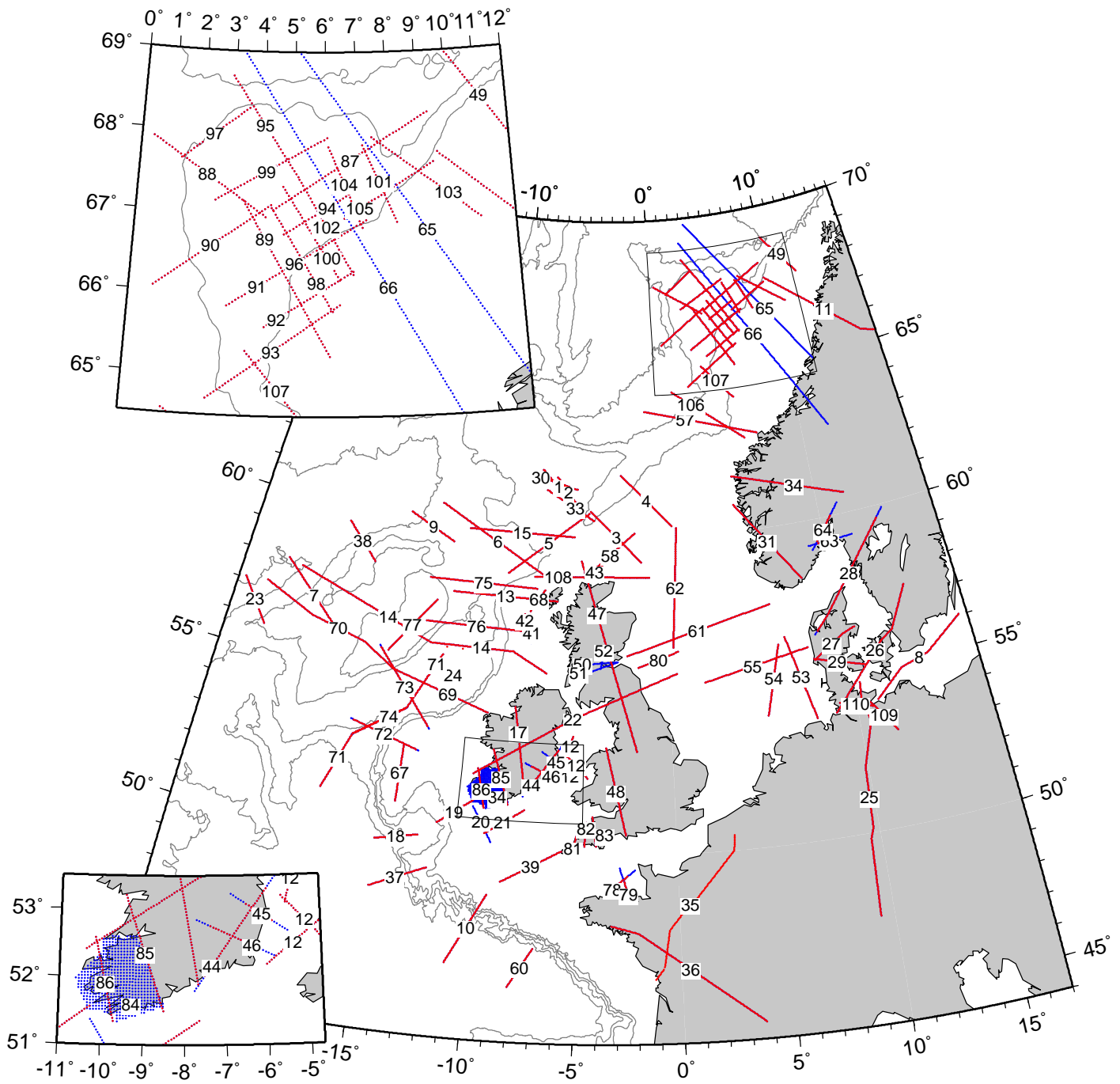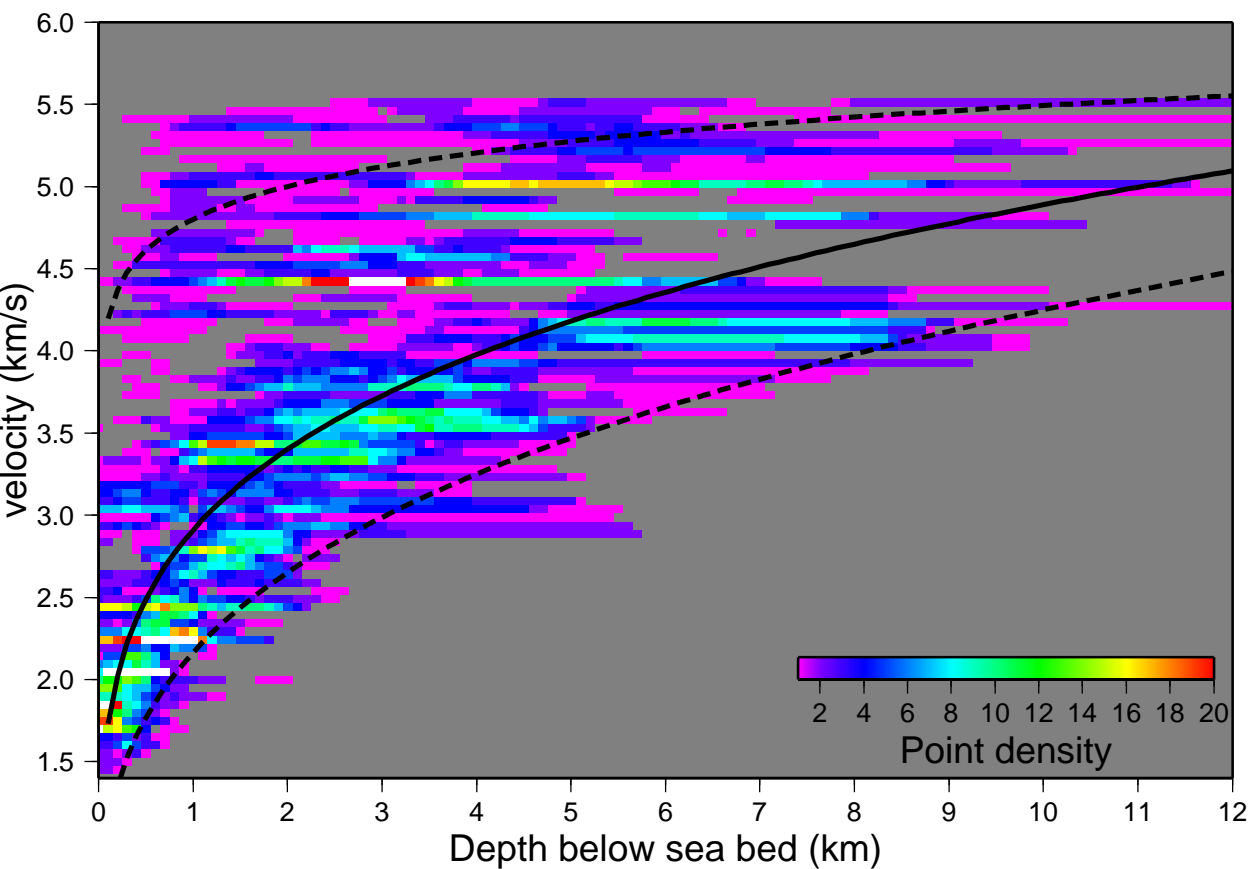
Figure 12. CRUST 2.0 model (after Bassin et al. 2000). The left-hand image a) is the mean velocity of the entire crust including sediments, the right-hand image b) is the mean velocity of the crystalline crust only.

Figure 13. Moho map of Western Europe, after Dezes and Ziegler (2004) for comparison with Fig. 9.
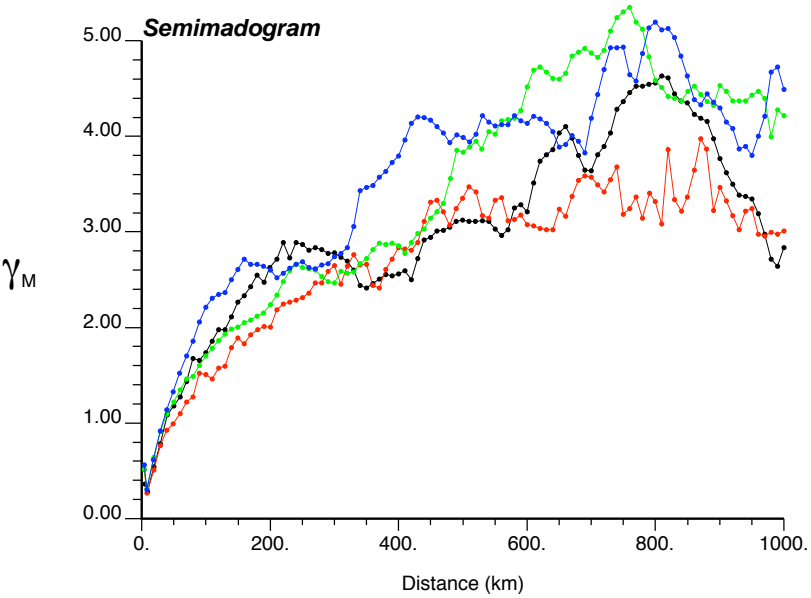
Table 1

Seismic reflection profiles used as a sources of data on P-wave velocity variation with depth in the sedimentary basins.

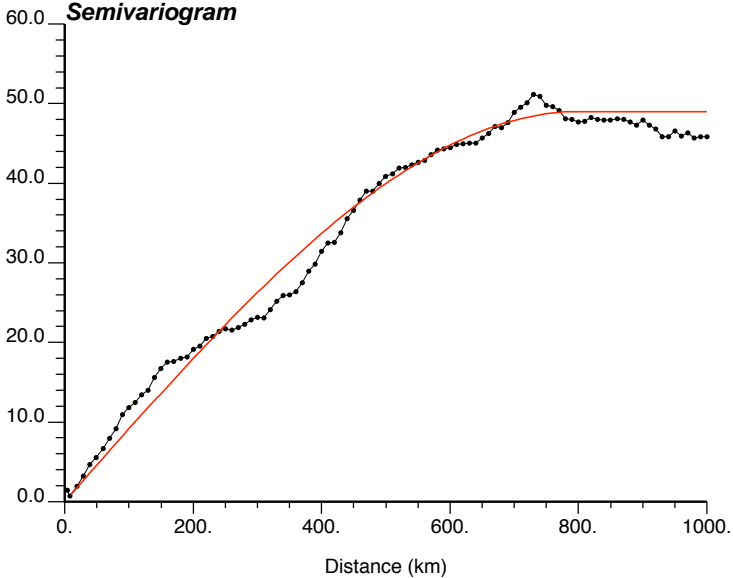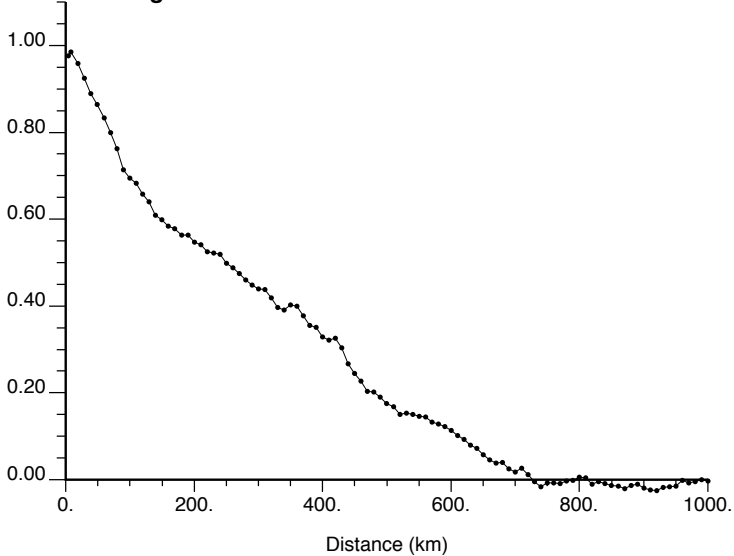| *Reflection profile*	*Location*
AMP Line L	Rockall Trough
AMP Line N	Porcupine Seabight
FAST	Faroe-Shetland Trough
AMP Line B	Faroe-Shetland Trough
AMP Line C	Faroe-Shetland Trough/northern North Sea
MONALISA 1	Southern North Sea
MONALISA 3	Southern North Sea
SWAT 4	Celtic Sea
SWAT 5	Celtic Sea

Semimadogram

γ_M (vertical axis, values 0.00 to 5.00)

Distance (km) (horizontal axis, values 0. to 1000.)

Semivariogram

γ

Distance (km)

Correlogram

ρ

Distance (km)

Horizontal

Dip = 30 degrees

Legend:
- 0
- 45
- 90
- 135
- 180
- 225
- 270
- 315
- Model

Distance (km)

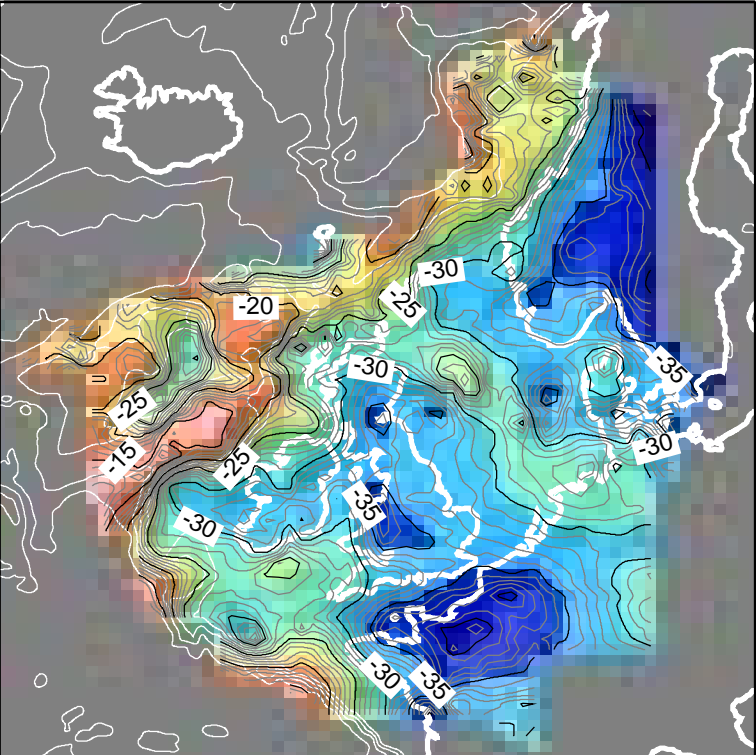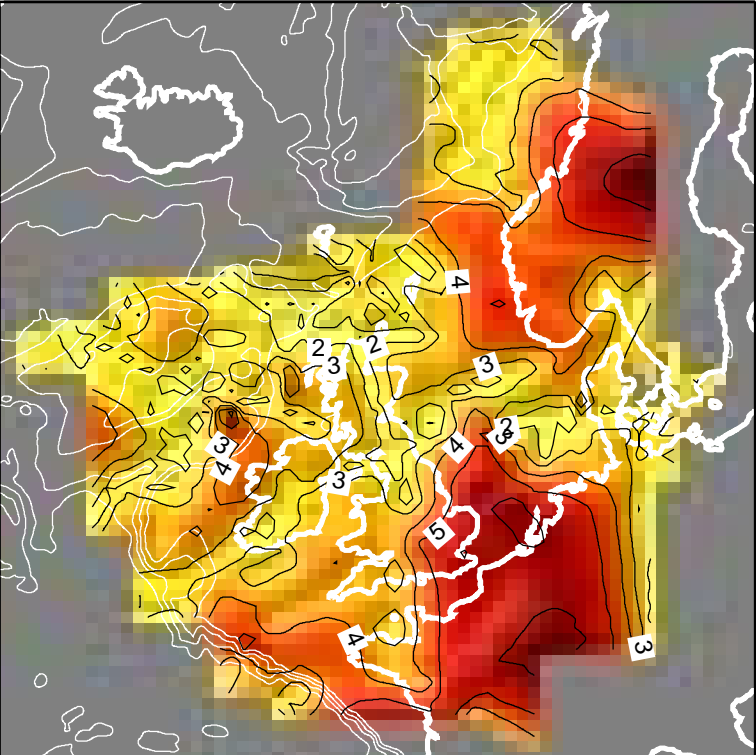**Dip = 60 degrees**

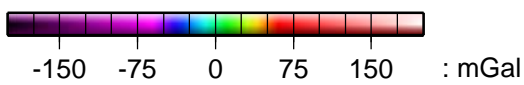Legend:
- 0
- 45
- 90
- 135
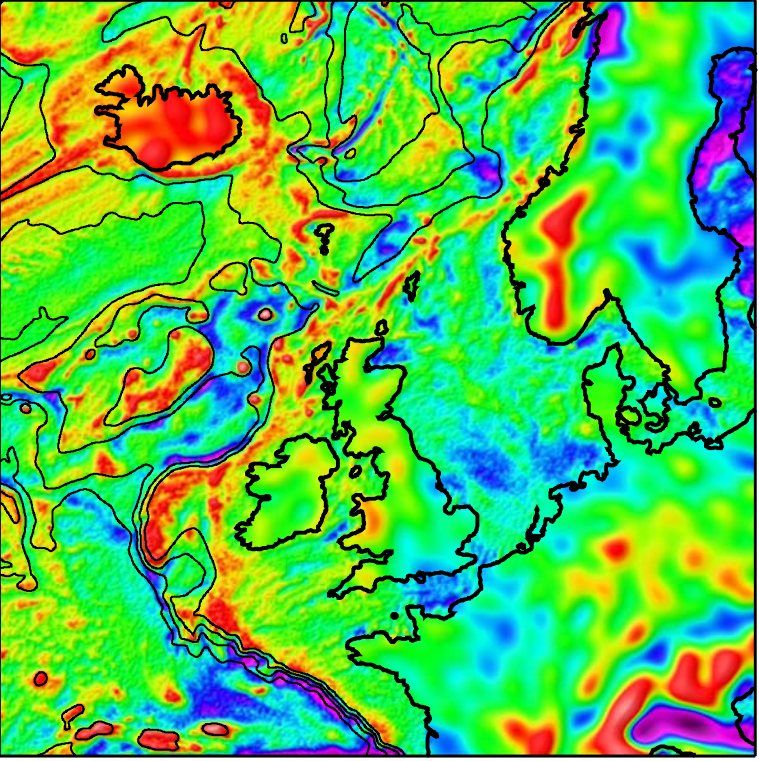- 180
- 225
- 270
- 315
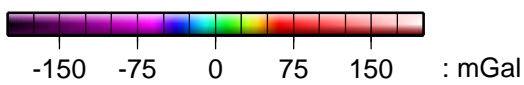- Model

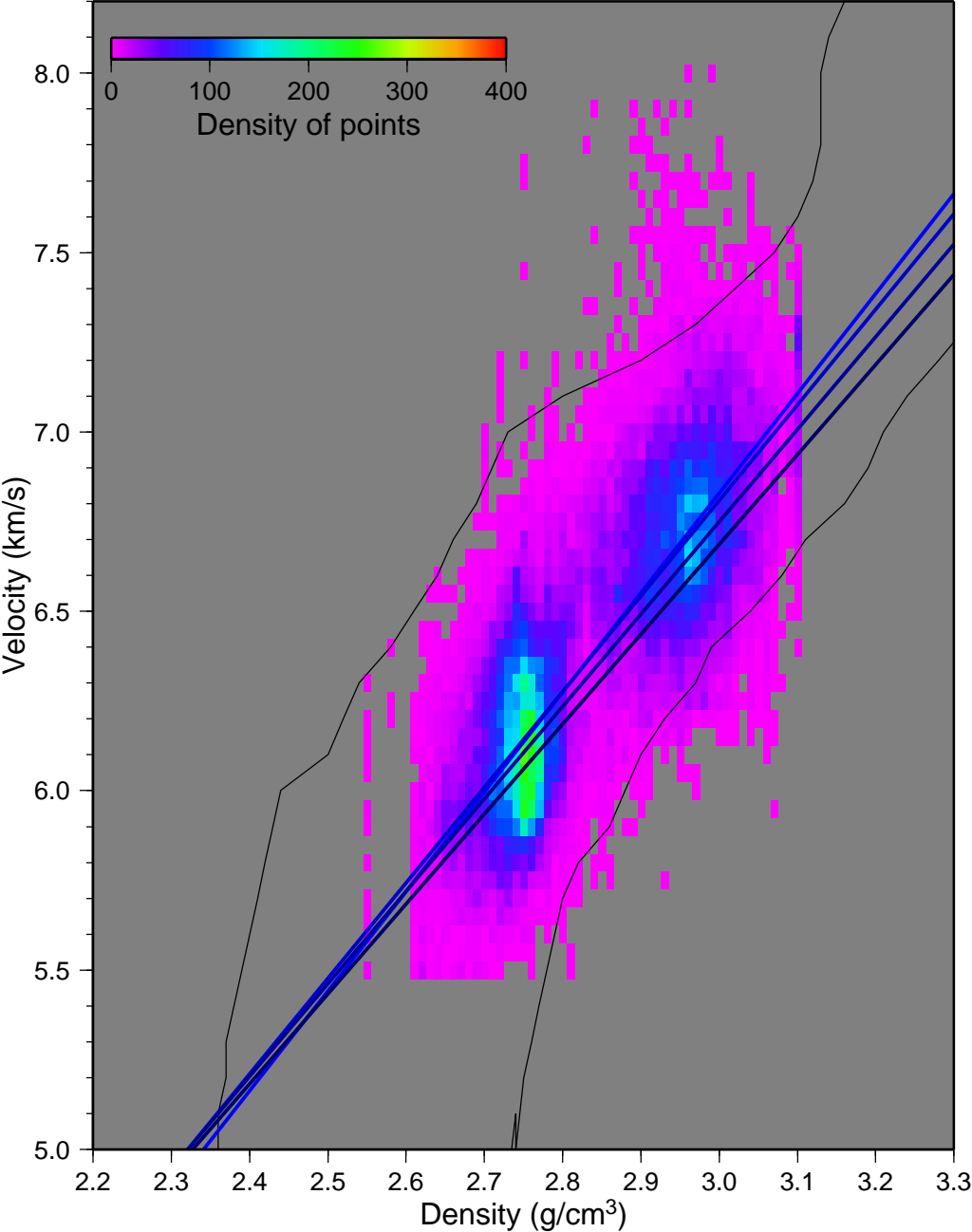X-axis: Distance (km)
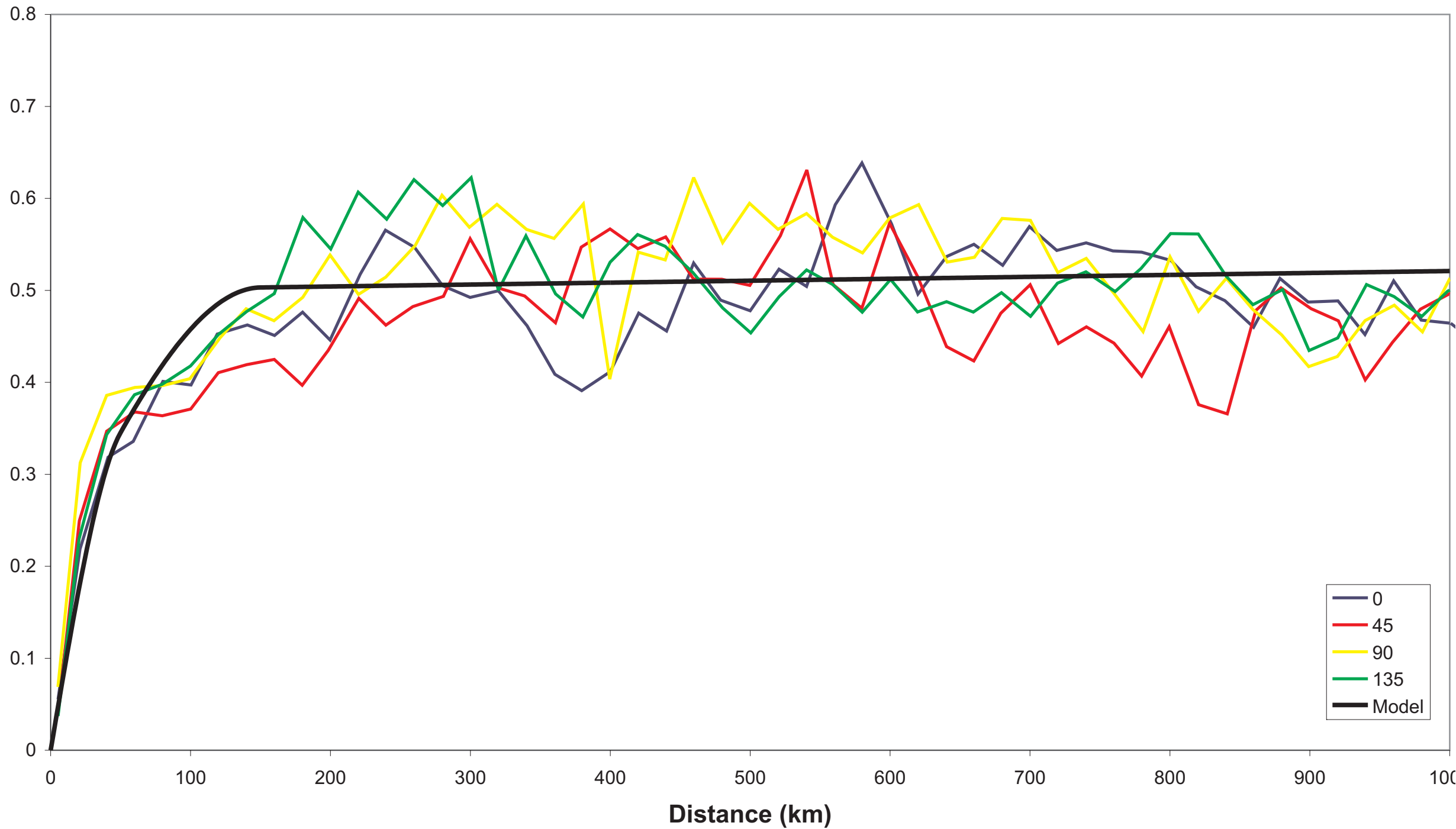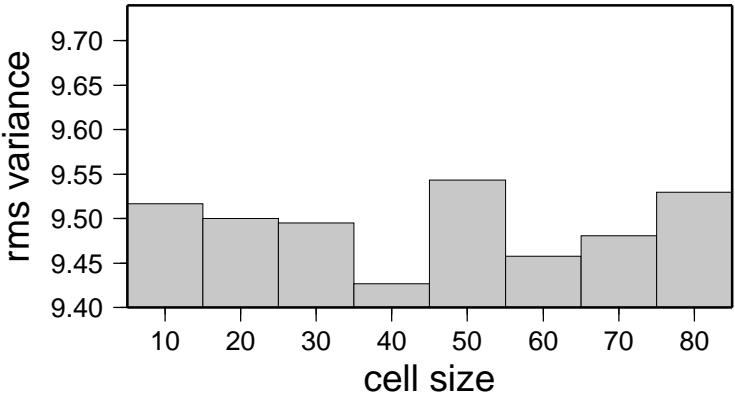
Interpolated Moho depth (km)
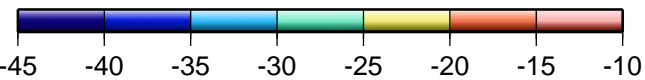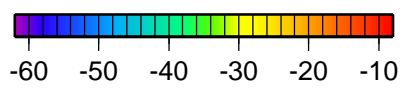
Moho depth uncertainty (km)

Observed Free Air Gravity

-150   -75   0   75   150   : mGal

Final Model: Calculated gravity anomaly

-150   -75   0   75   150   : mGal
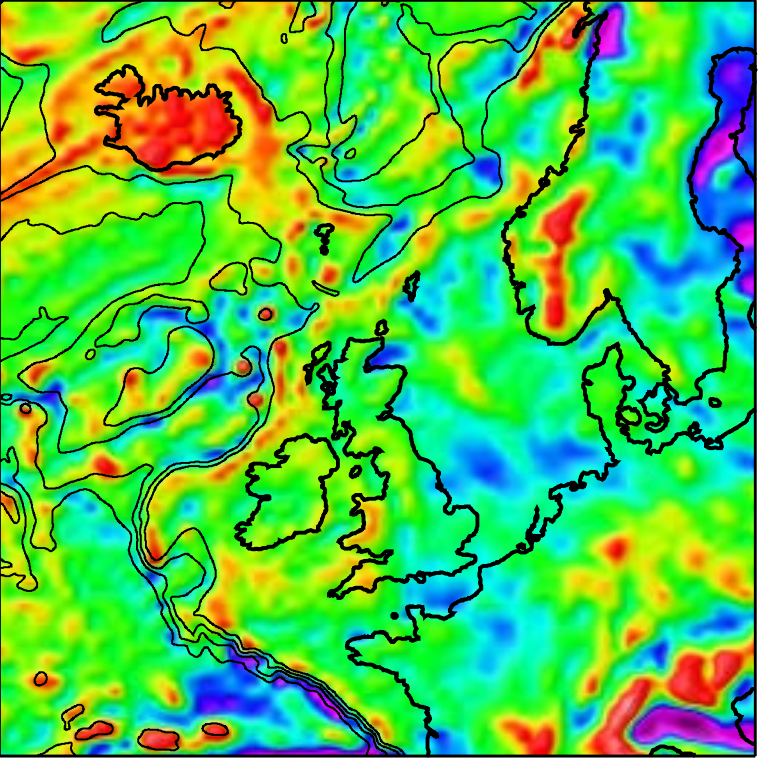
velocity-density pairs for the final model (by cell)

Moho Depth (km)
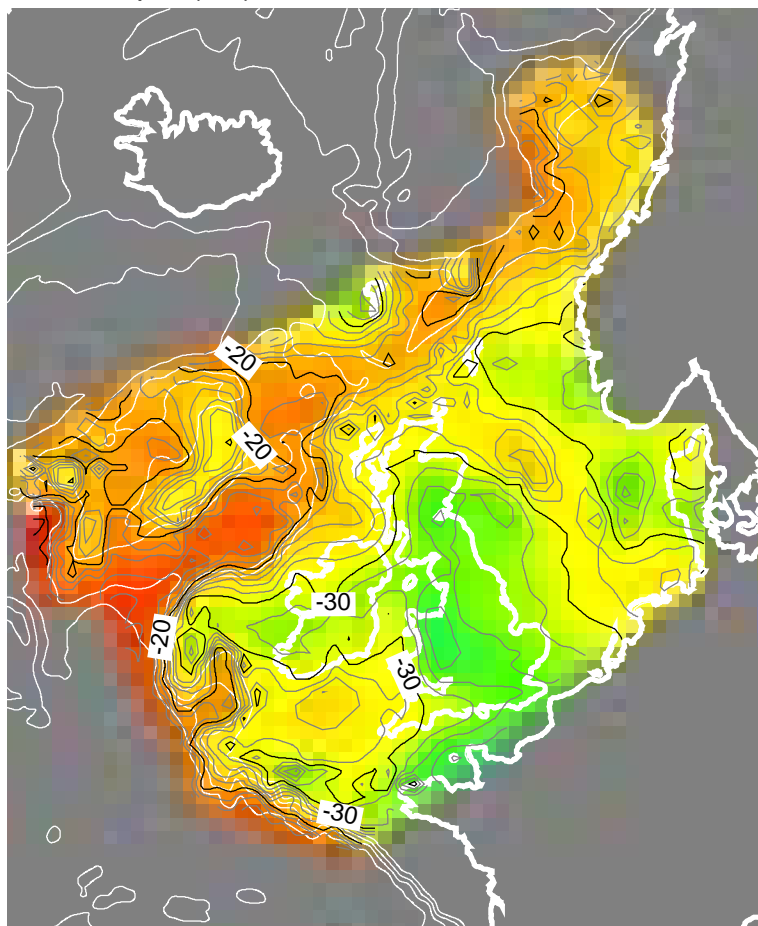
Velocity at -3.5 km below sea level (km/s)
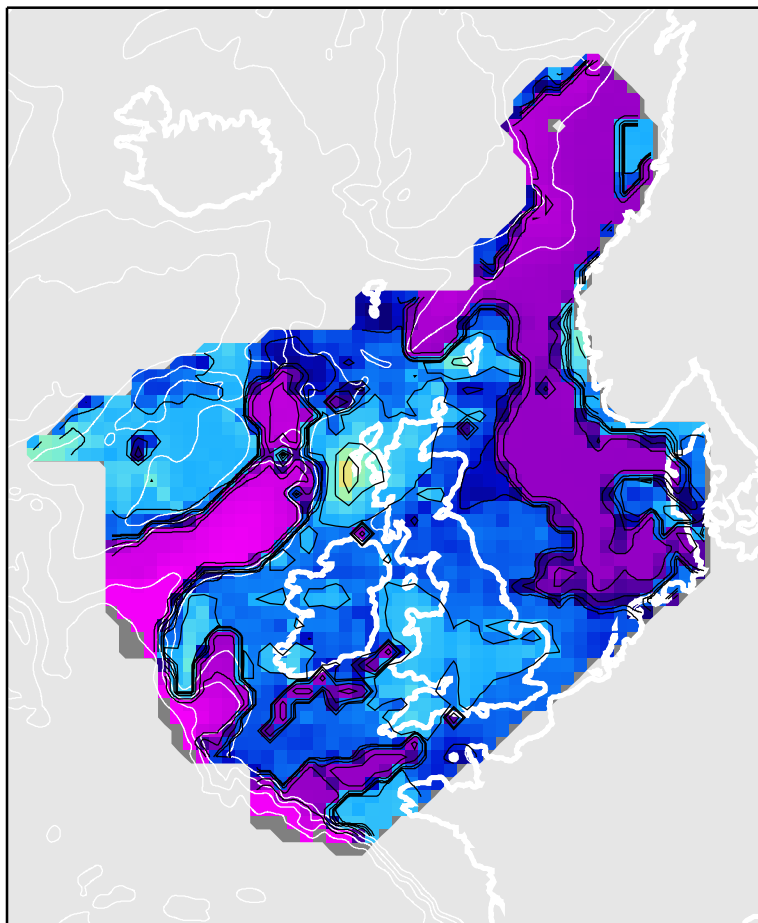
Vel uncertainty at -3.5 km below sea level (km/s)

Velocity at -6.5 km below sea level (km/s)

Vel uncertainty at -6.5 km below sea level (km/s)

Velocity at -17.5 km below sea level (km/s)

Vel uncertainty at -17.5 km below sea level (km/s)

Velocity at -26.5 km below sea level (km/s)
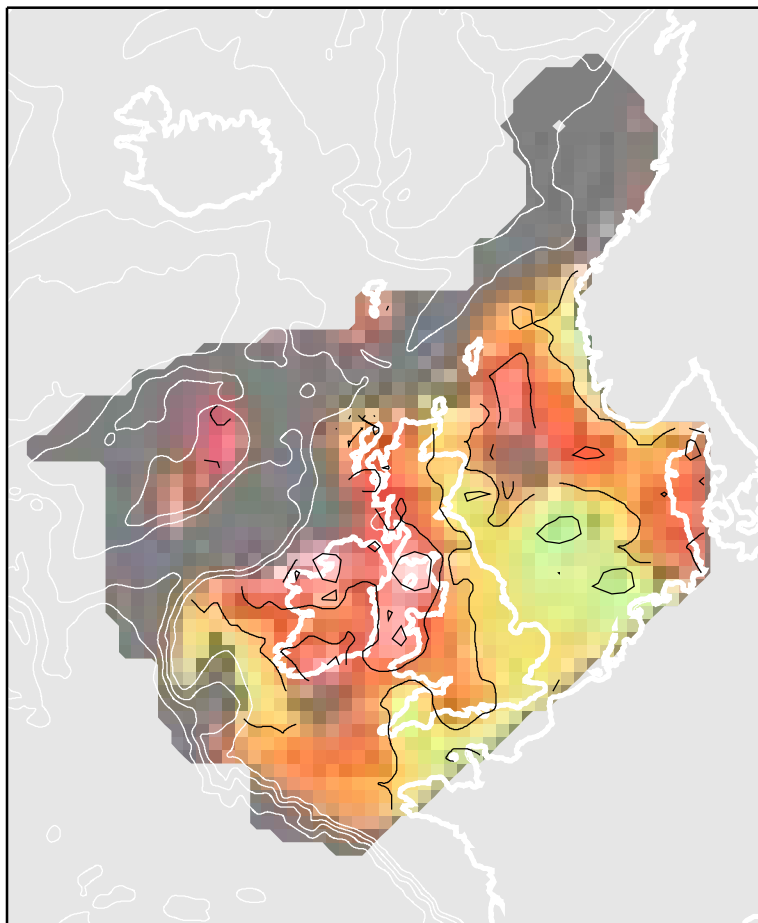
Vel uncertainty at -26.5 km below sea level (km/s)

velocity (km/s)

vel. uncertainty (km/s)

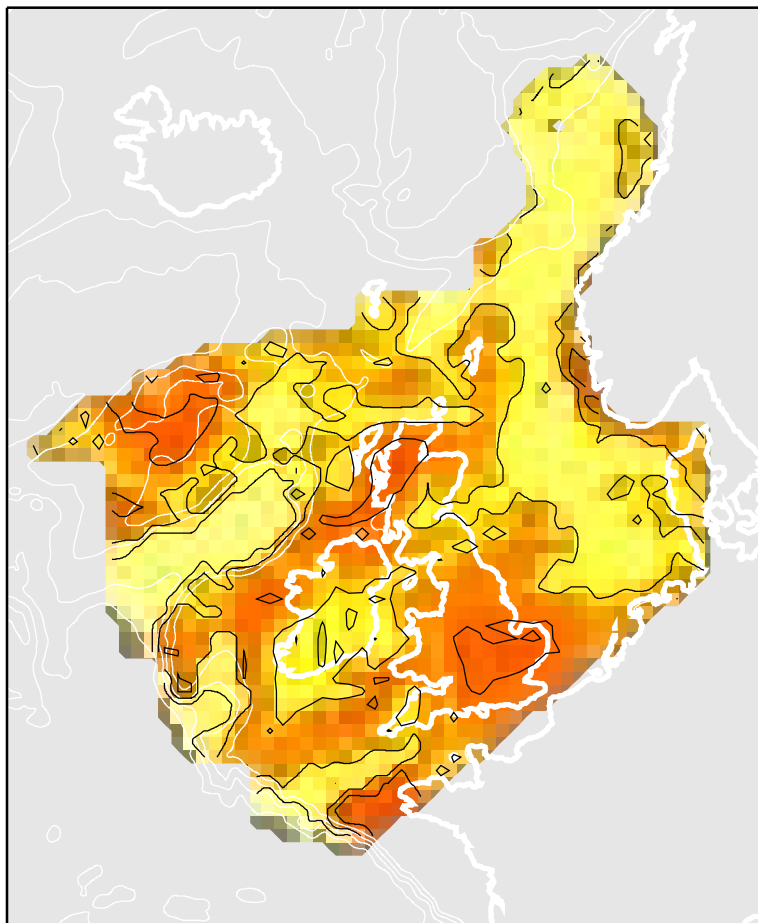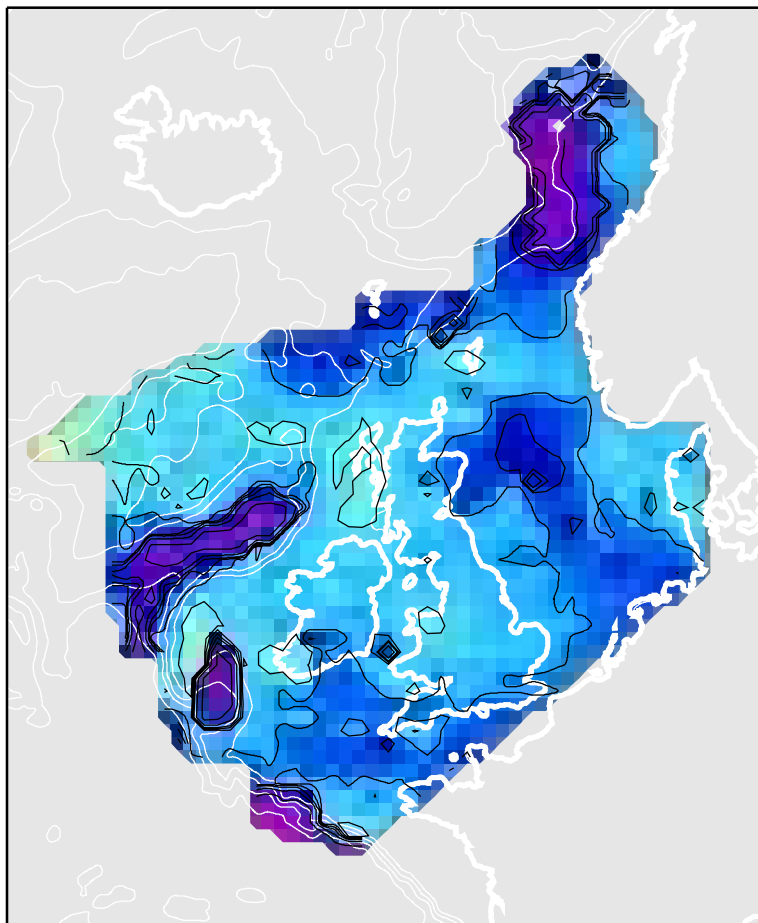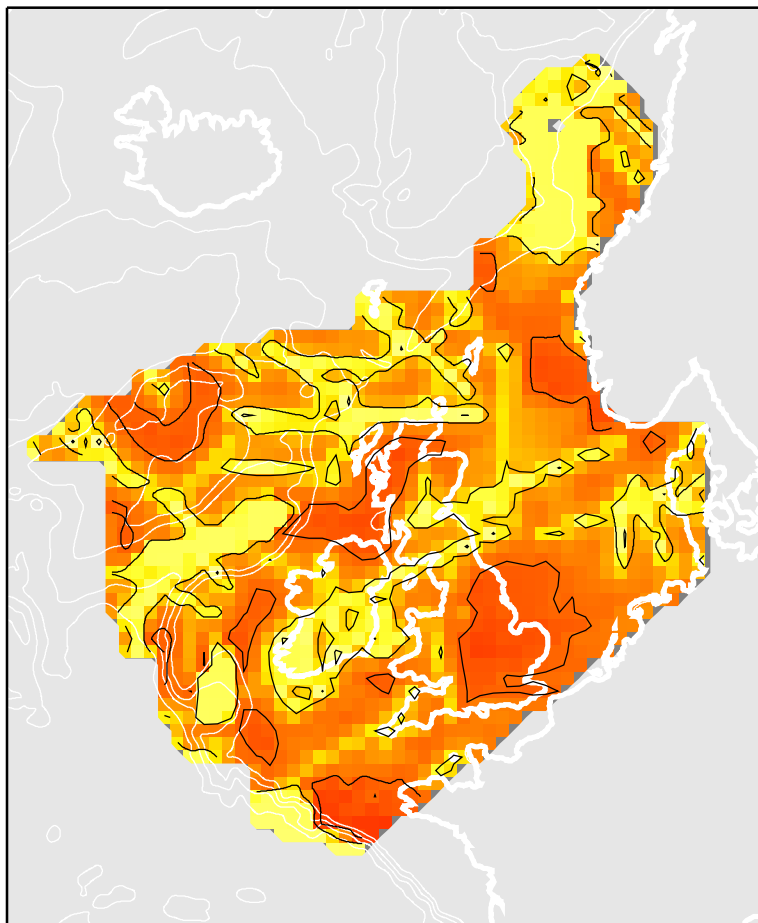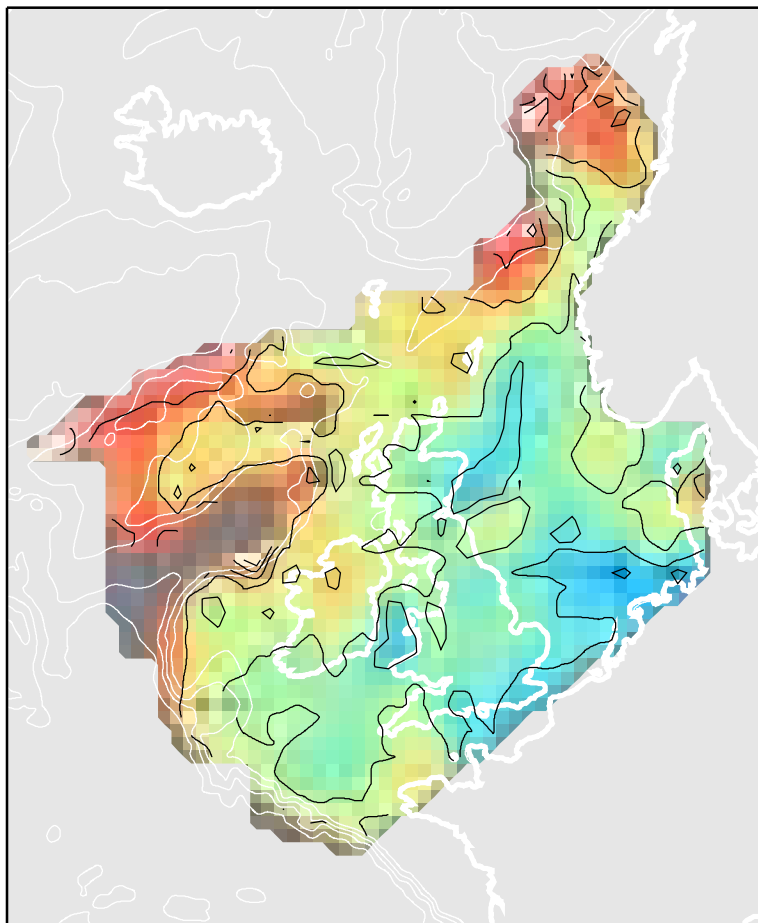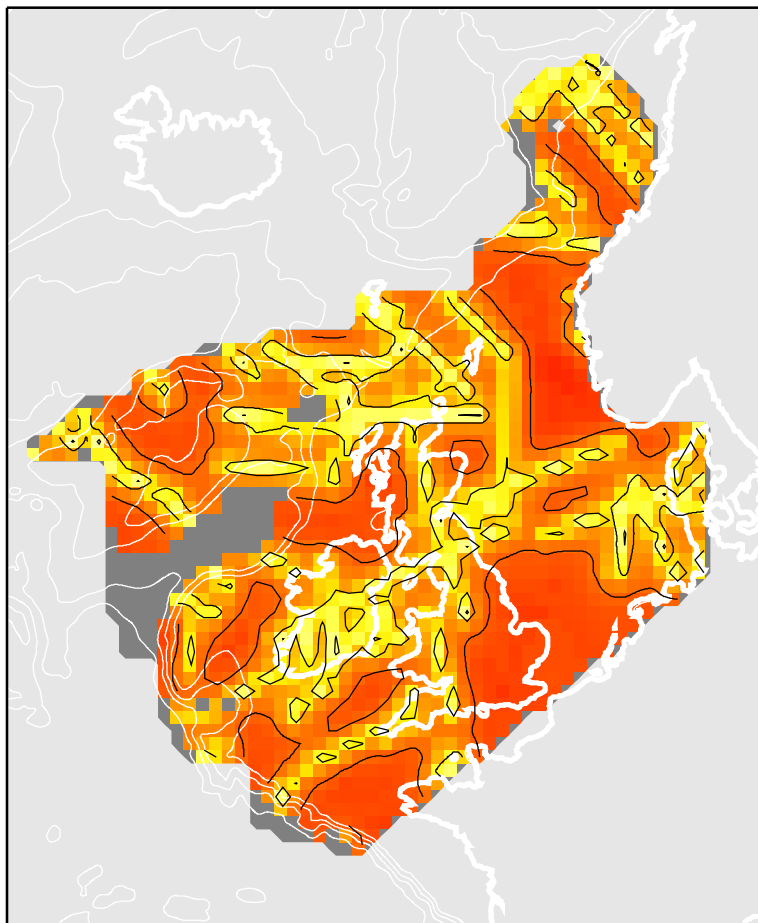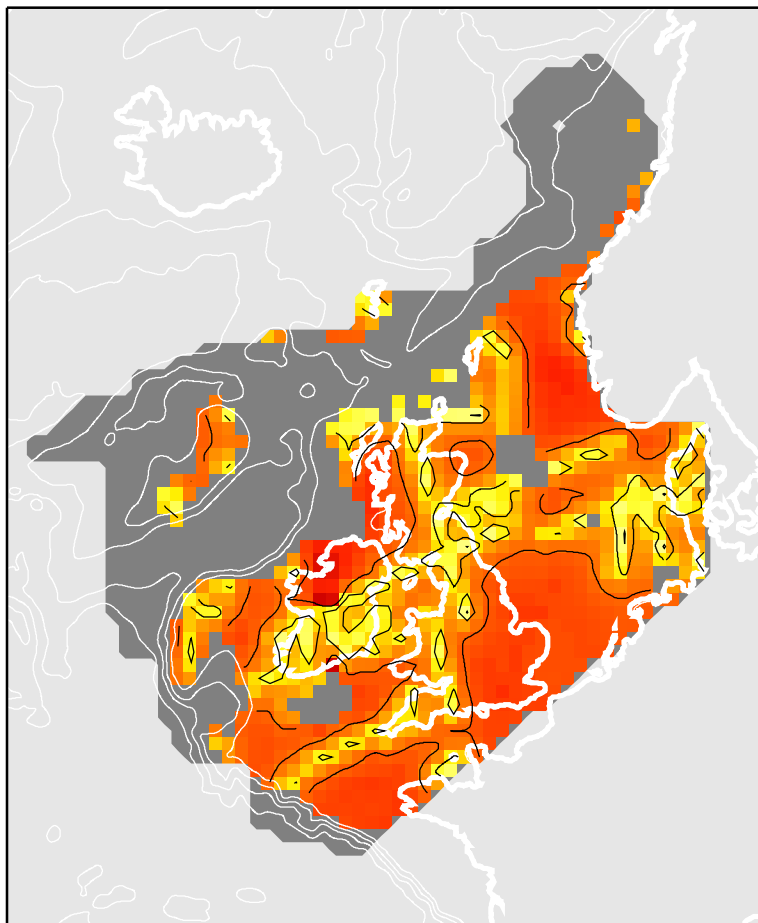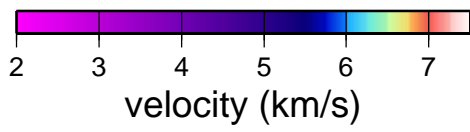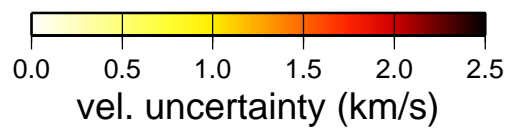Mean velocity (including sediments) (km/s)
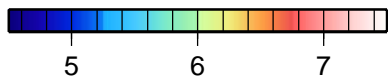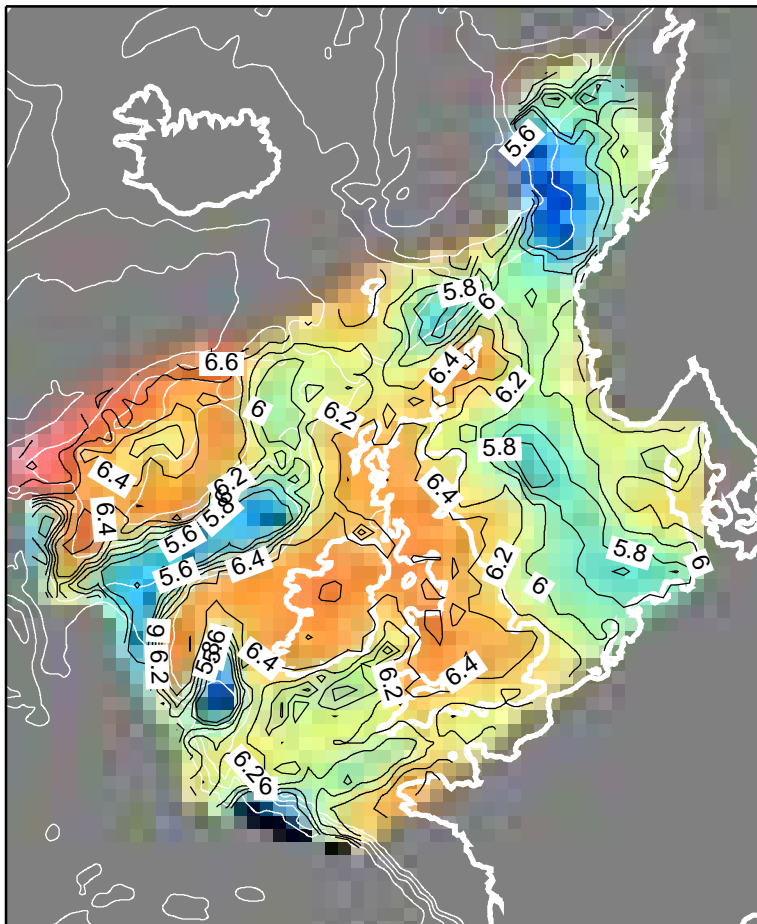
Mean velocity (excluding sediments) (km/s)
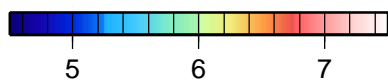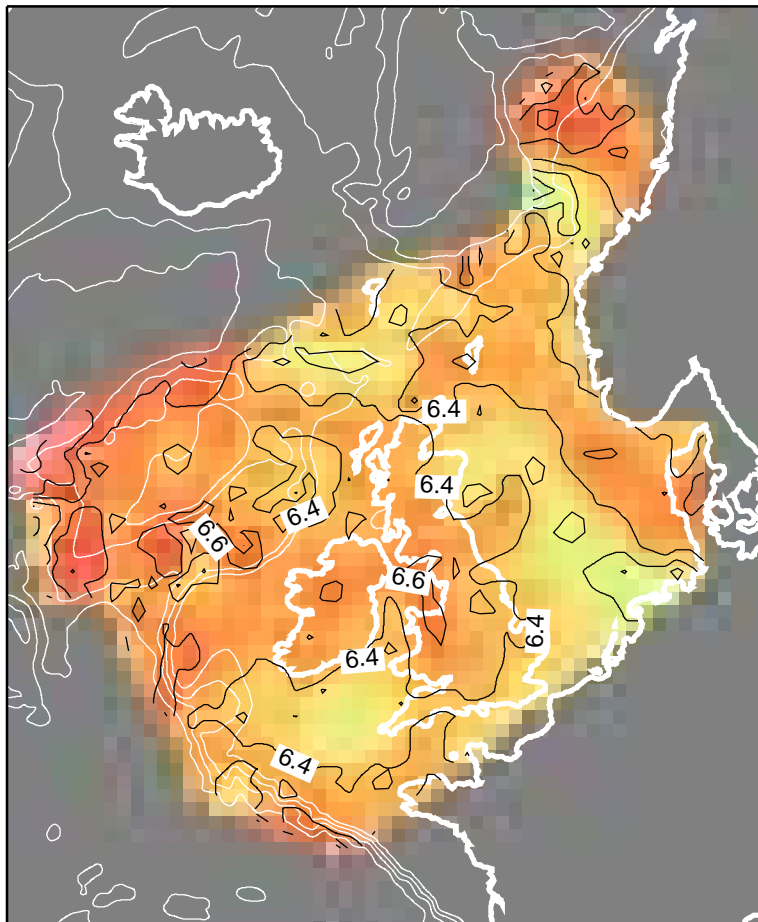
CRUST2.0 mean velocity (km/s)
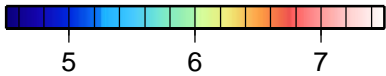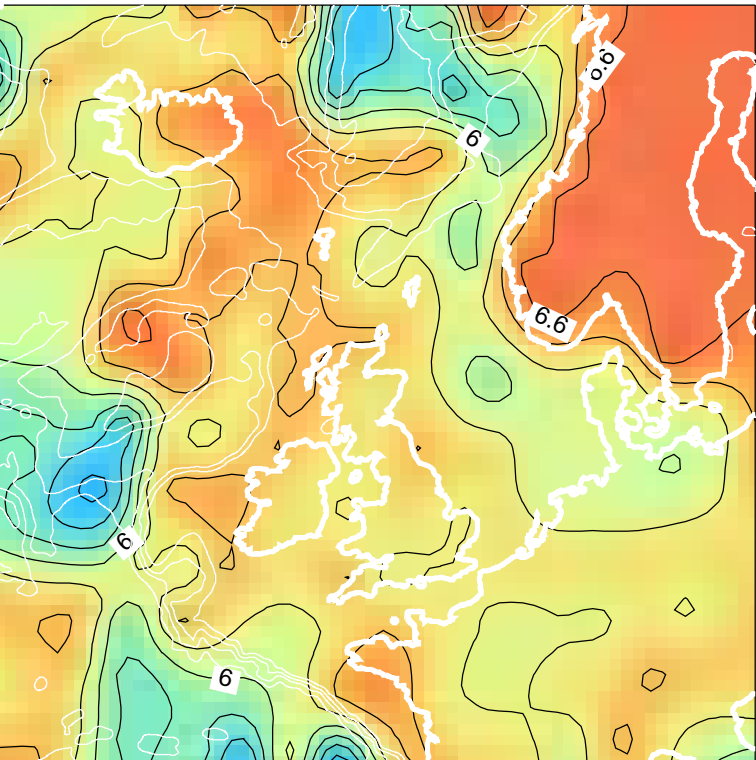
CRUST2.0 mean velocity (excluding sed) (km/s)
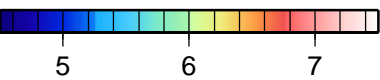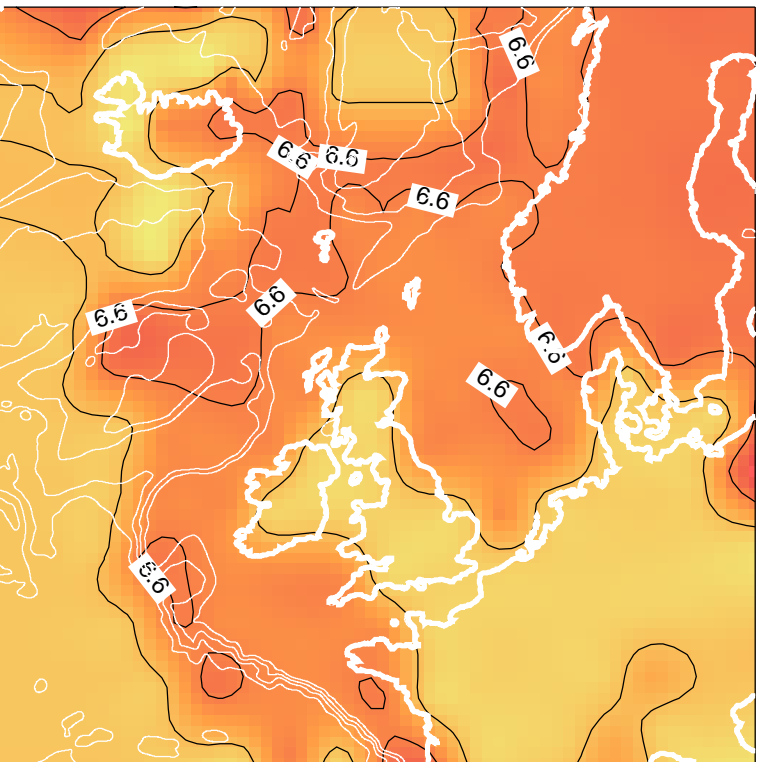
Map of the European Moho

Pierre Dèzes, Peter A. Ziegler

Universität Basel

EUCOR URGENT — UPPER RHINE GRABEN EVOLUTION & NEOTECTONICS

10 12 14 16 18 20 22 24 26 28 30 32 34 36 38 40 42 44 46 48 50 52 54 56 58 60 62 Kilometres

Projection: Lambert Azimuthal Equal Area; Centre: 04°.00"/48°.00"; Region : W/E/N/S = 350°/28°/62°/34°; Ellipsoide wgs-84
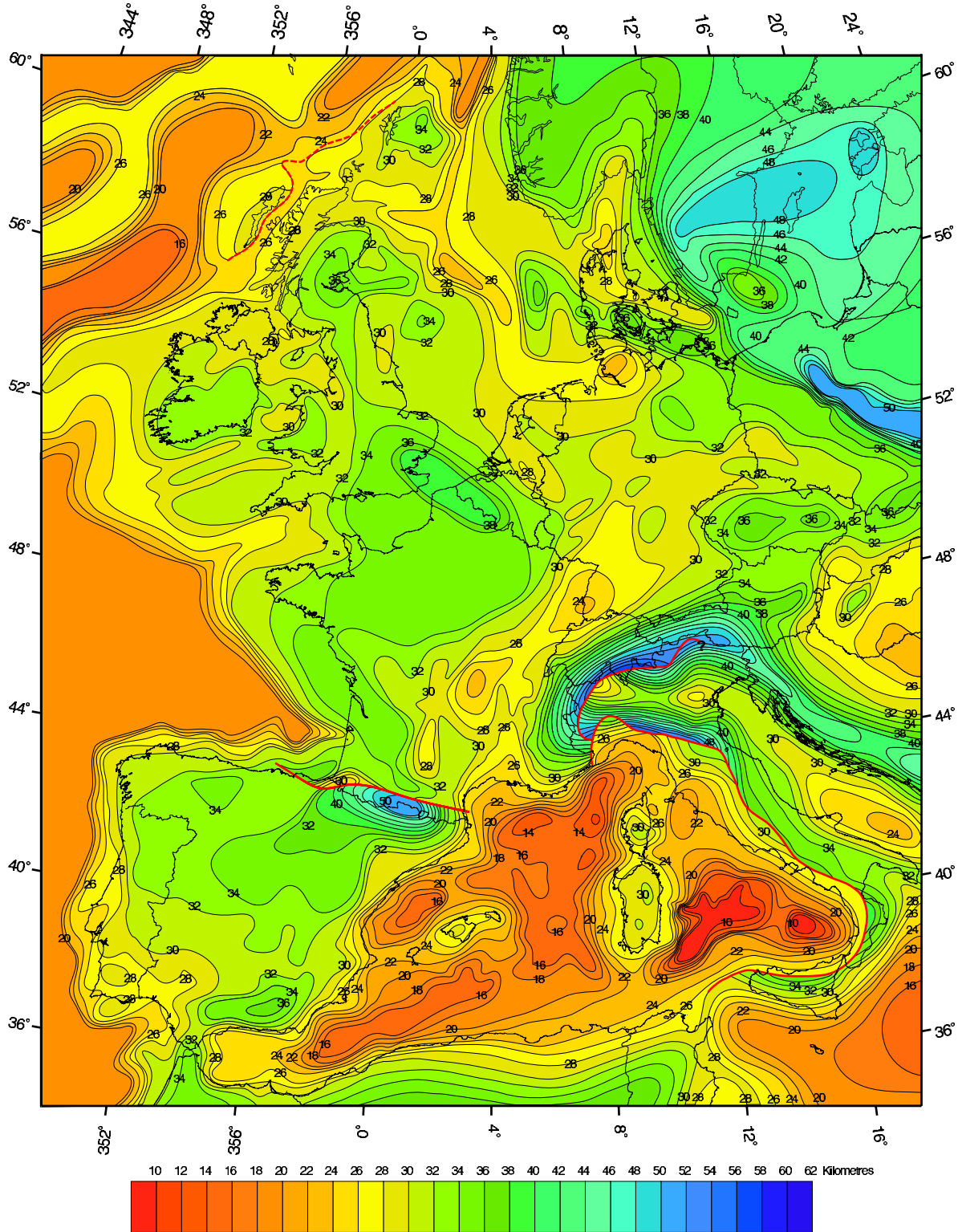
Depth to the Mohorovicic discontiunity, compiled with data from: Aljinovic et al. 1987; Ansorge et al. 1992; Argnani and Savelli 2001; Argnani and Torelli 2001; Arlitt et al. 1999; Blundell et al. 1992; Bois et al. 1994; Carrara 2001; Chadwick & Pharaoh, 1998; Chamot-Rooke et al. 1999; Chantraine et al. 1996; Cloetingh & Lankreijer 2001; Deichmann et al. 2000; Frasheri et al. 1996; Giese & Buness 1992; Hansen et al. 2000; Lekey 1999; Monaghan 2001; Morelli, 1998; Prodehl et al. 1995; Pfiffner et al. 1996; Rocca 2001; Rousset et al. 1993; Scarascia et al. 1994; Slejko et al. 1987; Skoko et al. 1987; Thybo et al. 1998; Torné et al. 1996; Van Wees 2000; Waldhauser 1998; Zeyen et al. 1997; Ziegler 1990

Appendix – Catalogue of wide-angle/refraction profiles used in the database

Listed below are the 2D wide-angle datasets used to build the database from which the 3D model was constructed. Also given are the known or estimated and assigned uncertainties in the depth to the Moho and the seismic velocities.

A.1 Moho Uncertainties

The following table catalogues the highest and lowest uncertainties assigned to the Moho input data. The first column of the table refers to the numbers on Fig. 1; the second column gives the profile name, if one is given in the publications; the third column contains the lowest uncertainty in km assigned to the Moho depth; the fourth column the highest uncertainty in km assigned to the Moho; and the fifth column the reference for the published models. The uncertainties are in italics if they have been taken from the original publication and in standard font if no uncertainties were provided, or the provided uncertainties have not been used.

No.	Name	Low	High	Reference
1	AMG95-FR1	*1*	*1*	Richardson (1997)
2	AMG95-FR3	*1.5*	*1.5*	Richardson (1997)
3	AMP-A	*0.5*	2	AMP Exclusive report 01/3/3 (2001)
4	AMP-C	*0.5*	2	AMP Exclusive report 01/3/3 (2001)
5	AMP-D	*0.5*	*1.5*	Klingelhöfer et al. 2005
6	AMP-E	*0.5*	*2.5*	Klingelhöfer et al. 2005
7	AMP-L	1	2.5	AMP Exclusive report 99/3/1 (1999)
8	BABEL-A	1	3	BABEL working group (1993)
9	BANS	*1.5*	*1.5*	Klingelhöfer et al. 2005
10	-	3	3	Ginzburg et al. (1985)
11	Blue-Norma	2	5	Avedik et al. (1984); Goldschmidt-Rokita et al. (1988)
12	-	3	3	Blundell and Parks (1969)
13	-	2	3	Bott et al. (1979)
14	CDP87	*1.5*	*1.5*	Klingelhöfer et al. 2005
15	CDP88	*1.5*	*1.5*	Klingelhöfer et al. 2005
17	COOLE	2	3	Lowe and Jacob (1989)
18	COOLE3a	2	2	Vogt (1993)
19	COOLE3b	2	2	Vogt (1993)
21	COOLE7	2	2	Vogt (1993)
22	CSSP	*1.3*	*2.5*	Al Kindi (2002)
23	-	1.6	1.6	Barton and White (1997)
24	-	*2*	*3*	Pearse (2002)
25	EUGEMI	1.5	2	Aichroth et al. (1992)
26	EUGENO-S1	1.5	3	EUGENO-S working group (1988)
27	EUGENO-S2	2	2	Thybo and Schonharting (1991)
28	EUGENO-S3	2	2	EUGENO-S working group (1988)
29	EUGENO-S5	1.5	3	EUGENO-S working group (1988)
30	FAST	*1*	*1.5*	Richardson (1997); Richardson et al. (1999)
31	-	4	4	Sellevoll and Warrick (1971)
33	FLARE	*2*	*2*	Richardson (1997); Richardson et al. (1999)
34	-	4	4	Sellevoll and Warrick (1971)
35	-	5	5	Matte and Hirn (1988)
36	-	3	5	Sapin and Prodehl (1973)
37	-	*1*	*2*	Horsefield et al. (1994)
38	-	1.5	2	Morgan et al. (1989)

39	-	3	3	Holder and Bott (1971)
42	-	5	5	Jones et al. (1984)
43	-	3	3	Jones et al. (1984)
44	LEGS-A	3	3	Hodgson (2002)
45	LEGS-B	3	3	Hodgson (2002)
46	LEGS-C	3	3	Hodgson (2002)
47	LISPB	1	1	Barton (1992)
48	LISPB-Δ	2	3	Bamford et al. (1976)
49	LOFOTEN	1.5	2	Goldschmidt-Rokita et al. (1988)
53	MONALISA1	1	3	Abramovitz and Thybo (1998)
54	MONALISA2	1	3	Abramovitz and Thybo (2000)
55	MONALISA3	1	5	Kelly (2006)
57	-	3	3	Eldholm and Grue (1994)
58	NASP-D	3	3	Smith and Bott (1975)
60	Norgasis	1	2	Thinon et al. (2003)
61	-	1	3	Barton and Wood (1984)
62	-	3	3	Christie (1982)
63	-	2	2	Tryti and Sellevoll (1977)
64	-	2	2	Tryti and Sellevoll (1977)
67	-	3	3	Whitmarsh et al. (1974)
68	PUMA	2	2	Powell and Sinha (1987)
69	RAPIDS1	2	4	O'Reilly et al. (1995)
70	RAPIDS13	*2*	*2*	Vogt et al. (1998)
71	RAPIDS2	1	1.5	Hauser et al. (1995)
72	RAPIDS32	1.5	2	Morewood et al. (2005)
73	RAPIDS33	1.5	2	Morewood et al. (2005)
74	RAPIDS34	1.5	2	Morewood et al. (2005)
75	Rockall 2	1	3	Roberts et al. (1988)
76	Rockall 5	1	3	Roberts et al. (1988)
77	-	1.5	1.5	Bunch (1979)
78	Siscad1	2	2	Grandjean et al. (2001)
79	Siscad2	2	2	Grandjean et al. (2001)
80	SWABS	1	3	McCaughey et al. (2000)
81	SWESE4	3	3	Brooks et al. (1984)
82	SWESE5	3	3	Brooks et al. (1984)
83	SWESE6	3	3	Brooks et al. (1984)
85	VARNETa	1	3	Landes et al. (2000)
86	VARNETb	1	3	Masson et al. (1998)
87	Vøring1-92	2	2	Mjelde et al. (1997)
88	Vøring1-96	2	2	Mjelde et al. (2001)
89	Vøring10-96	2	2	Raum et al. (2002)
90	Vøring11-96	2	2	Berndt et al. (2001)
91	Vøring12-96	2	2	Raum et al. (2002)
92	Vøring13-96	2	2	Raum et al. (2002)
93	Vøring14-96	2	2	Raum et al. (2002)
94	Vøring2-92	2.5	2.5	Mjelde et al. (1997)
95	Vøring2-96	2	2	Mjelde et al. (2001)
96	Vøring3-92	2.5	2.5	Mjelde et al. (1997)
97	Vøring3-96	2	2	Mjelde et al. (2001)
98	Vøring4-92	3	3	Mjelde et al. (1997)
99	Vøring4-96	2	2	Mjelde et al. (2001)

100	Vøring5-92	2.5	2.5		Mjelde et al. (1997)
101	Vøring5-96	2	2		Mjelde et al. (1998)
102	Vøring6-92	2.5	2.5		Mjelde et al. (1997)
103	Vøring6-96	2	2		Mjelde et al. (1998)
104	Vøring7-92	2.5	2.5		Mjelde et al. (1997)
105	Vøring7-96	2	2		Mjelde et al. (1998)
106	Vøring8a-96	2	2		Raum (2003)
107	Vøring9-96	2	2		Raum et al. (2002)
108	W reflector	1	1		Morgan et al. (2000)
109	ZIPE1	2	2		Rabbel et al. (1995)
110	ZIPE3	3	3		Rabbel et al. (1995)

A.2 Velocity Uncertainties

The following table catalogues the uncertainties assigned to the wide-angle refection velocity data. The first column of the table refers to the numbers on Fig. 1; the second column gives the profile name, if one is given in the publications; the third column gives a representative percentage uncertainty for the upper crust; the fourth contains a representative percentage uncertainty for the lower crust (if no value is present the profile does not provide constraints on lower crustal velocity structure; the fifth column gives a representative percentage uncertainty for the low velocity zones (if any exist in the model); and the sixth column gives the reference for the published models. The uncertainties are in italics if they have been taken from the original publication and in standard font if no uncertainties were provided, or the provided uncertainties have not been used.

No.	*Name*	*%*	*%*	*%*	*Reference*
1	AMG95-FR1	*8*	*7.5*	*23*	Richardson (1997)
2	AMG95-FR3	*5*	*11*	*20*	Richardson (1997)
3	AMP-A	*~1.5*	*~3*		AMP Exclusive Report 01/3/3 (2001)
4	AMP-C	*~1.5*	*~3*		AMP Exclusive Report 01/3/3 (2001)
5	AMP-D	1.5	3	15	Klingelhöfer et al. 2005
6	AMP-E	1.5	3	15	Klingelhöfer et al. 2005
7	AMP-L	1.5	3	15	AMP Exclusive Report 99/3/1 (1999)
8	BABEL-A	3	5		BABEL working group (1993)
9	BANS	2.5	4		Klingelhöfer et al. 2005
10	-	5	7		Ginzburg et al. (1985)
11	Blue-Norma	4.5	6		Avedik et al. (1984); Goldschmidt-Rokita et al. (1988)
12	-	7	10		Blundell and Parks (1969)
13	-	7	10		Bott et al. (1979)
14	CDP87	3	5		Klingelhöfer et al. 2005
15	CDP88	3	5		Klingelhöfer et al. 2005
17	COOLE	*~2*	5	15	Lowe and Jacob (1989)
18	COOLE3a	5	7		Vogt (1993)
19	COOLE3b	5	7		Vogt (1993)
20	COOLE6	5	-		Vogt (1993)
21	COOLE7	5	7		Vogt (1993)
22	CSSP	*~2.5*	*~7*		Al Kindi (2002)
23	-	*~1.5*	*~3*		Barton and White (1997)
24	-	*~12*	*~7.5*		Pearse (2002)
25	EUGEMI	3.5	5	20	Aichroth et al. (1992)
26	EUGENO-S1	4	6		EUGENO-S working group (1988)

27	EUGENO-S2	4	6		Thybo and Schonharting (1991)
28	EUGENO-S3	4	6		EUGENO-S working group (1988)
29	EUGENO-S5	4	6		EUGENO-S working group (1988)
30	FAST	*3*	*6*	*14*	Richardson (1997); Richardson et al. (1999)
31	-	10	12		Sellevoll and Warrick (1971)
33	FLARE	*6.5*	*25*	*6*	Richardson (1997); Richardson et al. (1999)
34	-	10	12		Sellevoll and Warrick (1971)
36	-	7	10	25	Sapin and Prodehl (1973)
37	-	~2	3.5		Horse.eld et al. (1994)
38	-	5	6		Morgan et al. (1989)
39	-	7	10		Holder and Bott (1971)
41	-	~4	12		Jones et al. (1984)
42	-	10	12		Jones et al. (1984)
43	-	10	12		Jones et al. (1984)
44	LEGS-A	4	6		Hodgson (2002)
45	LEGS-B	4	6		Hodgson (2002)
46	LEGS-C	4	6		Hodgson (2002)
47	LISPB	3	5		Barton (1992)
48	LISPB-Δ	6	8		Bamford et al. (1976)
49	LOFOTEN	4	6		Goldschmidt-Rokita et al. (1988)
50	MAVIS1	3.5	-		Dentith and Hall (1989)
51	MAVIS2	3.5	-		Dentith and Hall (1989)
52	MAVIS3	3.5	-		Dentith and Hall (1989)
53	MONALISA1	2	3		Abramovitz and Thybo (1998)
54	MONALISA2	2	3		Abramovitz and Thybo (2000)
55	MONALISA3	~3.5	~4		Kelly (2006)
57	-	5	6		Eldholm and Grue (1994)
58	NASP-D	7	10		Smith and Bott (1975)
59	Norddeutsch	5	7	20	Rabbel et al. (1995)
60	Norgasis	2.5	4		Thinon et al. (2003)
61	-	5	7		Barton and Wood (1984)
62	-	7	10		Christie (1982)
63	-	6	7		Tryti and Sellevoll (1977)
64	-	6	7		Tryti and Sellevoll (1977)
65	-	6	8		Planke et al. (1991)
66	-	6	8		Planke et al. (1991)
67	-	10	12		Whitmarsh et al. (1974)
68	PUMA	5	7		Powell and Sinha (1987)
69	RAPIDS1	3	4		Pearse (2002)
70	RAPIDS13	2.5	4		Vogt et al. (1998)
71	RAPIDS2	3	4		Hauser et al. (1995)
72	RAPIDS32	3	5		Morewood et al. (2005)
73	RAPIDS33	3	5		Morewood et al. (2005)
74	RAPIDS34	3	5		Morewood et al. (2005)
75	Rockall 2	3	5		Roberts et al. (1988)
76	Rockall	5	3	5	Roberts et al. (1988)
77	-	7	10	20	Bunch (1979)
78	Siscad1	5	7		Grandjean et al. (2001)
79	Siscad2	5	7		Grandjean et al. (2001)
80	SWABS	3	5		McCaughey et al. (2000)
81	SWESE4	7	10	20	Brooks et al. (1984)

82	SWESE5	7	10	20	Brooks et al. (1984)
83	SWESE6	7	10	20	Brooks et al. (1984)
84	VARNET3-D	*~3.5*	-		Landes et al. (2003)
85	VARNETa	3	5		Landes et al. (2000)
86	VARNETb	3	5		Masson et al. (1998)
87	Vøring1-92	3	5		Mjelde et al. (1997)
88	Vøring1-96	3	5		Mjelde et al. (2001)
89	Vøring10-96	3	5		Raum et al. (2002)
90	Vøring11-96	4	5		Berndt et al. (2001)
91	Vøring12-96	3	5		Raum et al. (2002)
92	Vøring13-96	3	5		Raum et al. (2002)
93	Vøring14-96	3	5		Raum et al. (2002)
94	Vøring2-92	3	5		Mjelde et al. (1997)
95	Vøring2-96	3	5		Mjelde et al. (2001)
96	Vøring3-92	3	5		Mjelde et al. (1997)
97	Vøring3-96	3	5		Mjelde et al. (2001)
98	Vøring4-92	4	6		Mjelde et al. (1997)
99	Vøring4-96	3	5		Mjelde et al. (2001)
100	Vøring5-92	3	5		Mjelde et al. (1997)
101	Vøring5-96	3	5		Mjelde et al. (1998)
102	Vøring6-92	3	5		Mjelde et al. (1997)
103	Vøring6-96	3	5		Mjelde et al. (1998)
104	Vøring7-92	3	5		Mjelde et al. (1997)
105	Vøring7-96	3	5		Mjelde et al. (1998)
106	Vøring8a-96	3	5		Raum (2003)
107	Vøring9-96	3	5		Raum et al. (2002)
108	W reflector	*~2*	*~1.5*		Morgan et al. (2000)
109	ZIPE1	4	6	15	Rabbel et al. (1995)
110	ZIPE3	5	7		Rabbel et al. (1995)